Title
A STUDY OF THE STRUCTURE AND COMPOSITION OF AN IRON SILICATE CATALYST, FEZSM-5, VIA ELECTRON MICROSCOPY

Author
Csencsits, R.

Publication Date
1988-11-01

Lawrence Berkeley Laboratory
UNIVERSITY OF CALIFORNIA

Materials & Chemical Sciences Division

National Center for Electron Microscopy

A Study of the Structure and Composition of an Iron Silicate Catalyst, FeZSM-5, Via Electron Microscopy

R. Csencsits
(Ph.D. Thesis)

November 1988

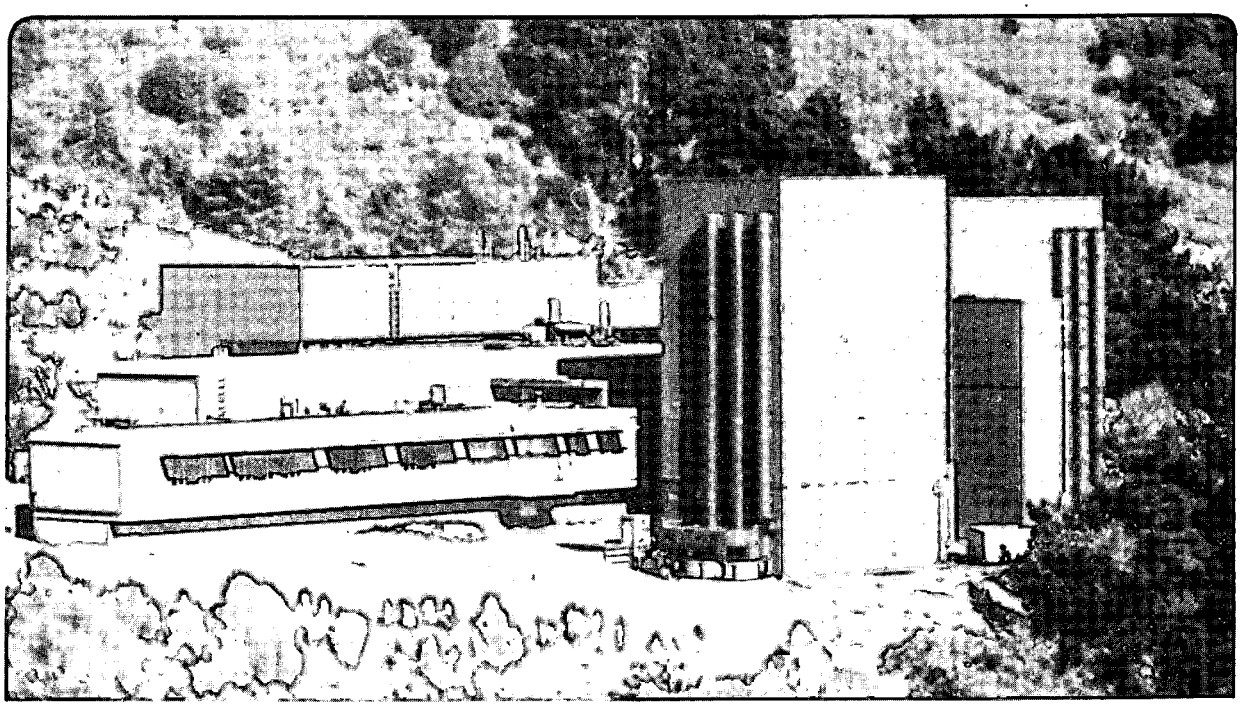

Prepared for the U.S. Department of Energy under Contract Number DE-AC03-76SF00098.

DISCLAIMER

A Study of the Structure and Composition of an Iron Silicate Catalyst, FeZSM-5, Via Electron Microscopy

Roseann Csencsits

Ph.D. Thesis
November 1988

Department of Materials Science and Mineral Engineering
University of California at Berkeley
and
Materials and Chemical Sciences Division
Lawrence Berkeley Laboratory
1 Cyclotron Road
Berkeley, CA 94720

This work was supported by the Director, Office of Energy Research, Office of Basic Energy Sciences, Materials Science Division of the U.S. Department of Energy under Contract No. DE-AC03-76SF00098.

A Study of the Structure and Composition of an Iron Silicate Catalyst, FeZSM-5, Via Electron Microscopy

Roseann Csencsits

Abstract

The purpose of this research is to understand the relationships between processing, structure, catalytic activity and selectivity of an iron silicate catalyst as a function of preparation and processing conditions. Iron silicate analogs of zeolite ZSM-5, referred to as FeZSM-5, represent the starting point for a novel method of dispersing catalytically active transition metals and transition metal oxides within the pores of a molecular sieve structure. The long term goal of iron silicate catalyst research is to synthesize a shape selective catalyst system; the promoted iron oxide is the active catalyst for the Fischer-Tropsch synthesis of hydrocarbons and the ZSM-5 structure would, by virtue of its pore size, restrict the products to the C_7-C_{10} "gasoline" range.

Scanning electron microscopy shows that stirring a gel of moderate to high iron concentration during crystal growth produces uniform, small iron silicate particles. Crystallization without agitation of the gel results in some small single crystals but predominantly large agglomerates of small crystallites are produced. Addition of alkali cations to the iron silicate gel during crystallization leads to a higher percentage of single, twinned and intergrown FeZSM-5 particles; however, most of the sample still consists of large particle agglomerates of small crystallites.

X-ray emission spectroscopy performed in the transmission electron microscope and in the scanning transmission electron microscope demonstrates that stirring the gel during crystal grow has a profound affect on the homogeneity of the iron distribution in the

FeZSM-5 particles.

The particle size and spatial distributions of the catalytic iron phase, determined using conventional transmission electron microscope imaging, are directly linked to the overall iron concentration in the sample as well as to the local distribution of iron prior to hydrothermal treatment. High resolution lattice imaging and microdiffraction techniques are used to identify some of the large iron-rich second phase particles as iron silicates, oxides and hydroxides.

A probe reaction, the dehydrogenation of ethyltoluene to methylstyrene, shows the FeZSM-5 catalysts to be both activity and shape selective. Although the Fischer-Tropsch synthesis using these catalysts is the subject of future work, this research has taken the first steps toward a promising future of shape selective iron silicate catalysts.

TABLE OF CONTENTS

CHAPTER 1

INTRODUCTION

1.1. Objective

The purpose of this research is to understand the structural and compositional changes of an iron silicate catalyst as a function of preparation and processing conditions. The relationship between synthesis conditions and the inter-particle and intra-particle compositional variations are determined; structural changes resulting from thermal and hydrothermal treatments are studied. Emphasis is placed on understanding the relationships between processing, structure, catalytic activity and selectivity.

1.2. Significance

The fine scale (0.5-10nm) structure and composition of a catalyst is vitally important to its activity and selectivity for a given reaction. These physical properties depend on the procedures used during the preparation of the catalyst. A correlation between the structural and compositional defects brought about by different synthesis and treatment schemes is desirable for the synthesis of improved catalysts.

1.3. Background

A catalyst is a material that facilitates the progress of a reaction to equilibrium without itself being consumed. This effect of catalysts is achieved by virtue of their unique surface characteristics. Catalyst sales in the United States net $1.5 billion every year. The revenue is spent almost equally on petroleum refining, chemical processing and emission control; however, the largest volume usage of catalysts is in the petroleum industry,

8.7 billion pounds of catalysts per year. Research and development of catalysts is aimed towards designing catalysts with superior activity and longer lifetimes.

Among the most important industrial catalysts are zeolites. Zeolites are crystalline alumino-silicates possessing regular and uniform pore structures. A general formula for zeolites is $M_{x/n}\,[(AlO_2)_x\,(SiO_2)_y]\;wH_2O$, where n is the valence of the cation M, x and y are the number of aluminum and silicon atoms, respectively, per unit cell and w is the number of water molecules occluded in the structure. Traditionally the nominal amount of aluminum in the zeolite is noted as its molecular SiO_2:Al_2O_3-ratio; this number is often noted in parentheses after the zeolite name, e.g., ZSM-5(50) is zeolite ZSM-5 with a SiO_2:Al_2O_3-ratio equal to 50:1.

The fundamental building block of zeolites is a tetrahedron of four oxygen anions surrounding a silicon or aluminum ion. These tetrahedra are arranged by sharing corners so that the zeolite has an open framework with a well defined pore structure. This open porous structure gives zeolites a very large internal surface area, $\sim$ 500 m^2/gm. It is the pore structure and high surface area that make zeolites particularly useful as catalysts and catalyst supports. A description of the various zeolite structures can be found in appendix I.

In the early 1970's researchers at Mobil Corporation synthesized a new shape selective zeolite catalyst, ZSM-5 with a unique channel structure that affords it unusual catalytic properties [1-5]. Zeolite ZSM-5 has orthorhombic symmetry [1] and cell parameters $a_o \sim 2.00$ nm, $b_o \sim 1.99$ nm and $c_o \sim 1.34$ nm. Its three dimensional channel system consists of straight channels parallel to [010] with ~ 0.54 nm $\times \sim 0.56$ nm diameter and sinusoidal channels parallel to [100] with ~ 0.51 nm $\times \sim 0.54$ nm free diameter [4] (figure 1.1). This small pore size prohibits the diffusion of large, highly branched organic

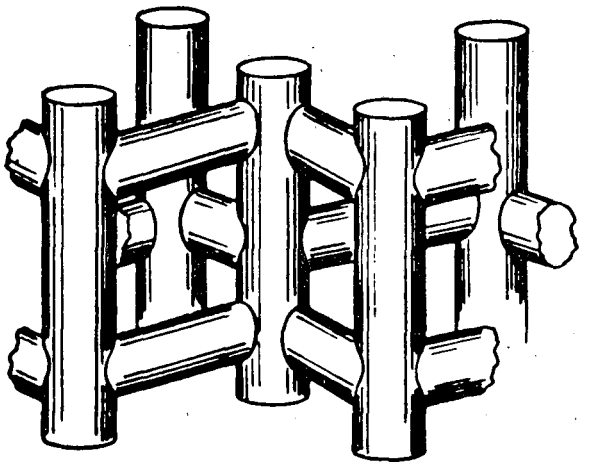

XBL 886-2080

Figure 1.1 - The channel structure in ZSM-5. [1]

molecules while allowing rapid diffusion of smaller straight chain organics. New petroleum refining and petrochemical processes [6] such as distillate dewaxing, paraffin cracking, xylene isomerization, and the conversion of methanol to gasoline are now possible because of shape selective zeolites.

After the successful conversion of methanol to gasoline, Mobil researchers also tested the ability of zeolite ZSM-5 to control the products of the Fischer-Tropsch reaction by reacting CO and H_2 over the physical mixture of catalytically active iron and ZSM-5 powder [7-9]. The results were very promising. Throughout the eighties, researchers worldwide have been trying to optimize the distribution of catalytically active iron and ZSM-5 to produce a better Fischer-Tropsch catalyst [10-13].

Iron silicate analogs of ZSM-5, referred to as FeZSM-5, represent the starting point for a novel method of dispersing catalytically active transition metals and transition metal oxides within the pores of a molecular sieve structure. The long term goal of iron silicate catalyst research is to synthesize a shape selective catalyst system, iron oxide

dispersed *inside* the pores of the ZSM-5 structure, that is active for direct conversion of carbon monoxide and hydrogen to gasoline range hydrocarbons. The promoted iron oxide is the active catalyst for the Fischer-Tropsch synthesis of hydrocarbons, and the ZSM-5 structure would, by virtue of its pore size, restrict the products to the C_7-C_{10} gasoline range. The reader is referred to reference [14] for a review of Fischer-Tropsch synthesis.

Iron silicate molecular sieves are crystallized in an autoclave from gels prepared by titrating a basic silica solution into an acidic iron solution followed by introduction of a crystal directing agent or template, usually tetrapropylammonium ions (TPA) [13, 15]. The resulting structure is analogous to zeolite ZSM-5 with iron occupying the framework sites usually occupied by aluminum, and the nominal amount of iron in the structure is noted by the SiO_2:Fe_2O_3-ratio, directly analogous to the SiO_2:Al_2O_3-ratio for zeolites. Sodium ions and the TPA ions are closely associated with the iron for charge neutrality. The TPA ions are subsequently removed by calcination (heat treatment in dry atmosphere). This thermal treatment also moves some of the framework iron atoms into non-framework sites. The catalytically active iron oxide particles grow as more iron moves out of the framework during subsequent hydrothermal treatments [15- 17]. The size and location of the oxide particles depend on the conditions of the steaming and on the initial SiO_2:Fe_2O_3-ratio of the FeZSM-5 particles.

In the FeZSM-5 catalysts, the catalytic activity is linked to the iron oxide particle surface while the shape selectivity results from the ZSM-5 pore structure. The amount of iron oxide available for reaction is very important; if particles grow very large the surface/volume ratio decreases and many iron atoms are wasted because they are not accessible. Therefore the size distribution of iron oxide particles is important in analyzing catalytic activity data. The location of iron oxide particles, internal or external surfaces

of the molecular sieve, will influence the product distribution of a reaction; thus knowing the spatial distribution of the iron oxide with respect to the ZSM-5 framework would aid in interpreting product distributions in terms of shape selectivity. The size of iron oxide particles depends on the temperature and duration of the steam treatments as well as the initial SiO_2:Fe_2O_3-ratio during growth of the FeZSM-5 crystals [17]. This thesis additionally postulates that the particle size and particularly the spatial distribution of the iron oxide are dependent on the concentration of iron and its gradients in the ZSM-5 framework before thermal and hydrothermal treatments, which would depend on the growth conditions, particularly the SiO_2:Fe_2O_3-ratio of the gel and whether the gel is stirred during crystal growth. The size and spatial distributions of the catalytic iron oxide particles could also have a strong influence on the shape selectivity, particularly if the catalytic phase is on the external surface of the molecular sieve thereby eliminating the shape selectivity of the reaction. Additionally, if the iron oxide is on the external surface of the ZSM-5 crystal then it could grow quite large in size thus reducing its surface/volume-ratio and therefore its catalytic activity.

This electron microscopy study is aimed at understanding factors that influence the activity and shape selectivity of these iron silicate catalysts. How does stirring the gel during crystal growth and the gel SiO_2:Fe_2O_3-ratio affect the size and shape of the FeZSM-5 particles and how do they affect the homogeneity of the iron concentration in the FeZSM-5 particles before heat treatment? What is the particle size and spatial distributions of iron oxide in the FeZSM-5 catalysts after calcination and various steam treatments? Is the iron oxide in fact an oxide, or is it a hydroxide or an iron silicate? And finally, how does the size and spatial distribution of this second phase affect the catalytic activity and shape selectivity of the FeZSM-5 ?

1.4. Technical Approach

Researchers in Dr. Rosemarie Szostak's group at the Georgia Institute of Technology synthesize, process and catalytically evaluate the FeZSM-5 catalysts. Structural and compositional characterization on the micron and nanometer scales are carried out in the electron microscopes at the Lawrence Berkeley Laboratory, the University of California at Berkeley, and at the Bethlehem Steel Company.

Scanning electron microscopy (SEM) is used to determine the size and morphology of the FeZSM-5 particles. X-ray emission spectroscopy (XES) performed in the transmission electron microscope (TEM) and in the scanning transmission electron microscope (STEM) is used to study the homogeneity of the iron throughout the catalyst particles before steam treatments. The particle size and spatial distributions of the catalytic iron phase are determined using conventional TEM imaging and their identity is studied with high resolution lattice imaging and microdiffraction techniques.

CHAPTER 2

PARTICLE SIZE AND MORPHOLOGY OF FeZSM-5

The particle sizes and morphologies of FeZSM-5 as a function of various preparatory conditions, thermal and hydrothermal treatments are studied using scanning electron microscopy.

2.1. Background: the scanning electron microscope

This section gives a brief description of the scanning electron microscope (SEM) and the reader is referred to references [18- 20] for more detail. Figure 2.1 shows a schematic representation of a conventional SEM. Electrons from a filament are accelerated by a voltage of 10-30 kV down an electron optical column. Two condenser lenses and an objective lens focus the electrons to a fine probe on the specimen surface. Scanning coils located above the objective lens cause the probe to raster the specimen surface in a square raster pattern, while the screen of a cathode ray tube (CRT) is scanned synchronously. While scanning, the electron beam interacts with the specimen creating a variety of signals (backscattered, Auger and secondary electron, cathodoluminescence and X-rays) that may be used for image formation and analysis. Secondary electrons have low ($<$50 eV) energy and are characteristic of the surface at the particular point of emission. These secondary electrons are picked up by a slightly (positive) biased detector. The small positive bias attracts the low energy Auger and secondary electrons but not the high energy ($\leq$ 10 keV) backscattered electrons; the Auger electrons are a very low energy, low intensity signal and only produce a negligible background to the secondary electron signal. The signal from the secondary electrons is amplified and is converted to a voltage that

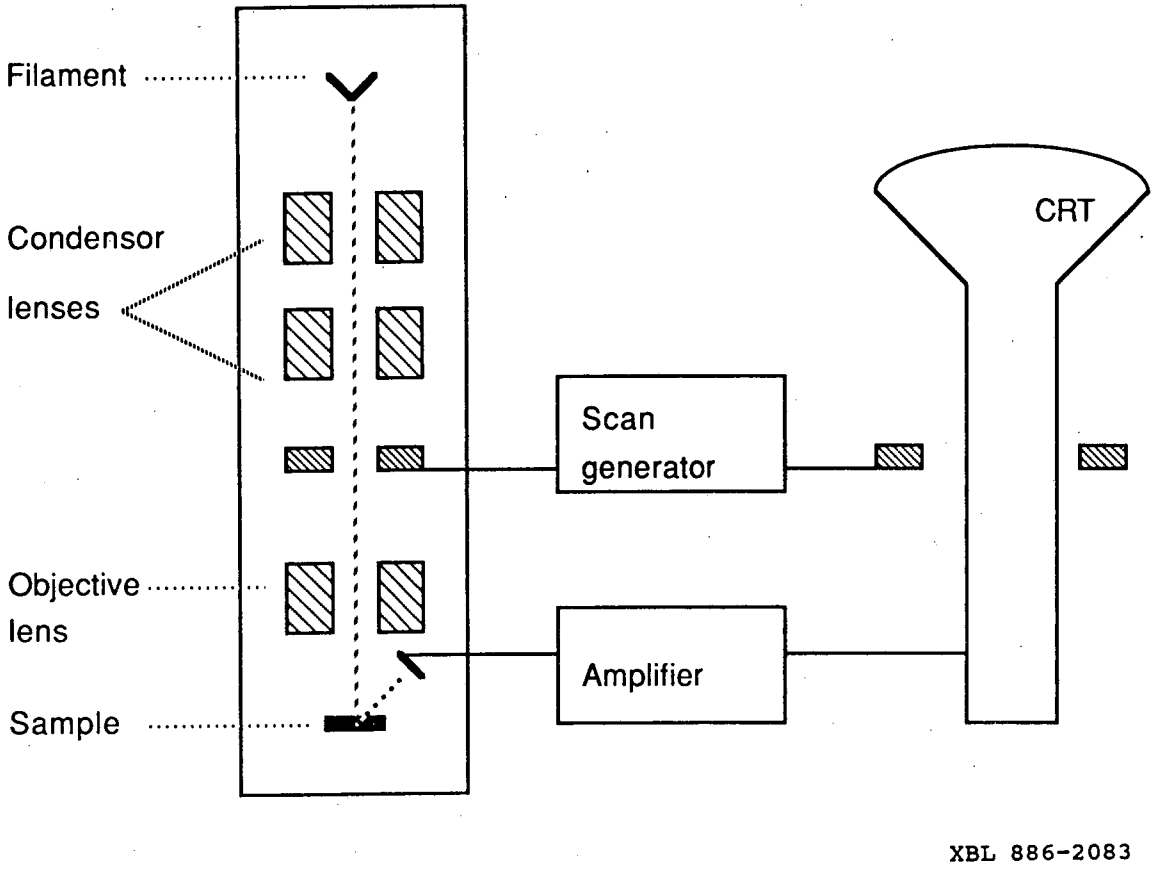

Figure 2.1 - Schematic diagram of a scanning electron microscope.

modulates the brightness of the spot on the CRT. The brightness of the spot is controlled by the current of secondary electrons reaching the collector. Variations in composition, texture and topography are monitored as changes in the brightness of the CRT spot. The picture, therefore, is a picture of the specimen surface. Since the size of the raster scanned on the specimen surface is much smaller than the size of the raster of the CRT, the final picture is a magnified image of the surface of the specimen.

2.2. Specimen preparation

Powder samples of FeZSM-5 were mounted on the SEM stubs with "TV tube koat", a suspension of carbon in a volatile organic solvent. After drying in air for 24 hours, the samples were sputter coated with 25 to 27 nm of platinum to prevent charging under the electron beam. Observations were carried out in the ISI DS-130 scanning electron microscope with a lanthanum hexaboride filament.

2.3. Results and discussion

2.3.1. Effects of stirring and iron concentration

Samples of FeZSM-5 grown from stirred and unstirred gels with SiO_2:Fe_2O_3-ratios $\simeq$ 50, 90 and 200, corresponding to 4, 2, and 1 iron atoms per unit cell of ZSM-5, respectively, are examined in the as-synthesized, heat and steam treated forms. Particles grown from stirred gels with high iron content, SiO_2:Fe_2O_3-ratios $\simeq$ 50, form complex "cauliflower-shaped" aggregates of smaller crystallites, shown in figure 2.2. As the iron concentration in the gel mixture decreases the particle aggregates became more regularly shaped, usually forming cuboidal or spherical agglomerates; these agglomerates are generally less than 1μm diameter (fig. 2.3).

Unstirred gels produce a few single crystals of FeZSM-5 and a variety of twinned and inter-grown crystals, but predominantly the samples are comprised of 2-5μm diameter aggregates of smaller molecular sieve particles (fig. 2.4). Decreasing the iron concentration in the gel from SiO_2:Fe_2O_3 $\simeq$ 50 to SiO_2:Fe_2O_3 $\simeq$ 200 results in more single crystals, approaching a ~~couple~~ few percent of the sample but generally the samples contain larger spherical particle aggregates, some larger than 5μm in diameter.

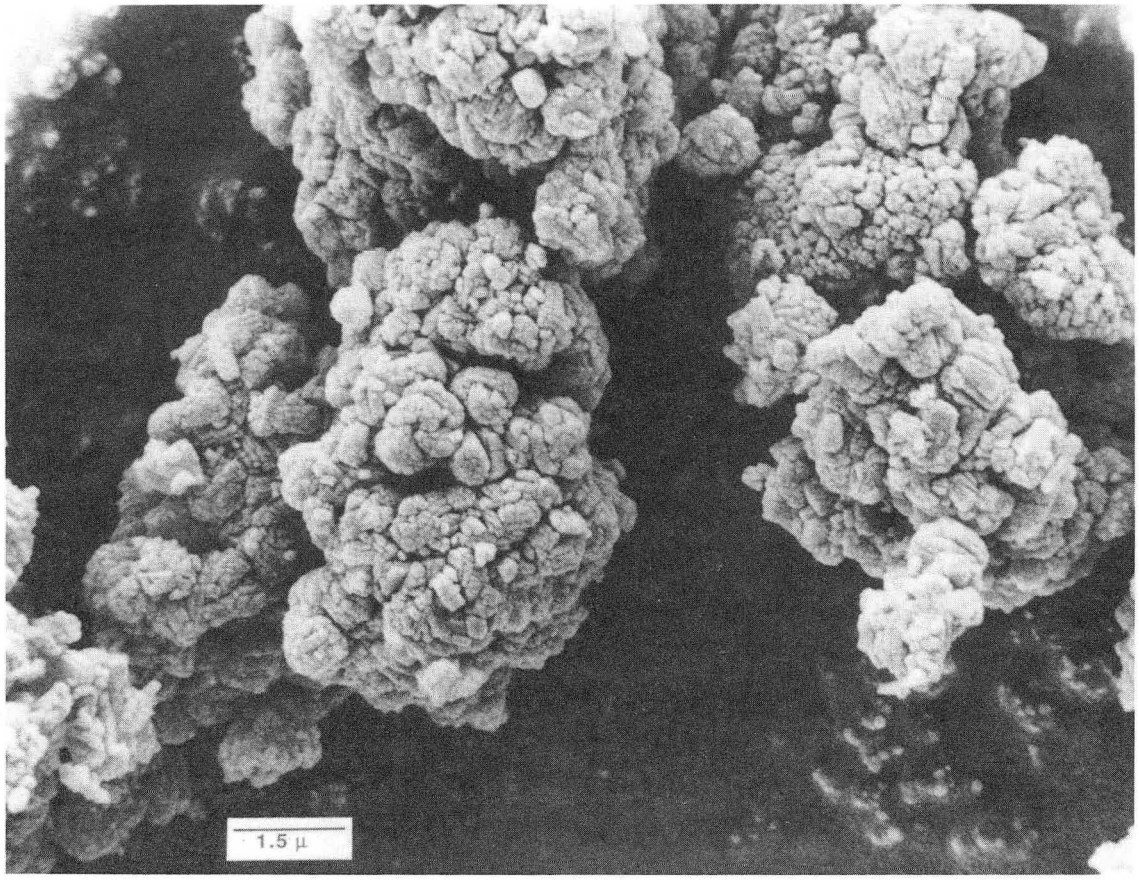

Figure 2.2 - SEM image of iron silicate molecular sieve in the as-synthesized form, grown from a stirred gel with SiO_2:Fe_2O_3-ratio $\simeq$ 50 showing "cauliflower-shaped" particle aggregates. XBB 8711-10115

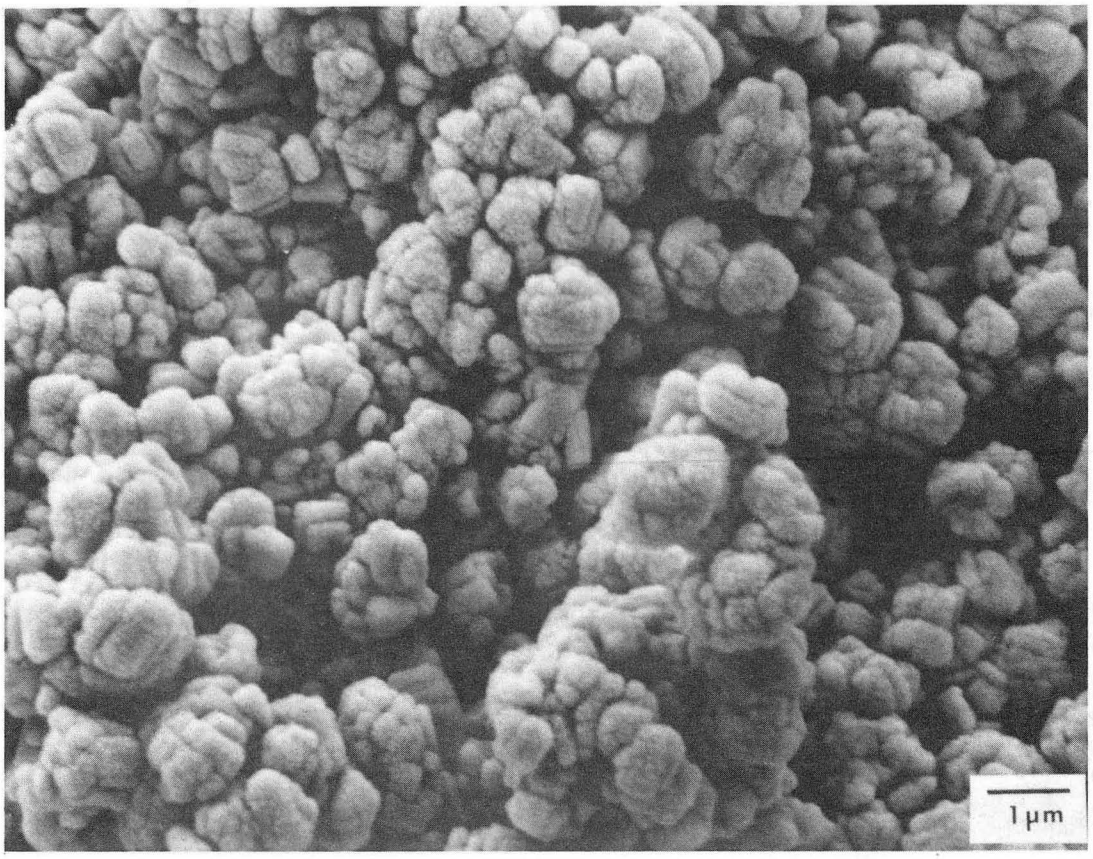

Figure 2.3 - SEM image of FeZSM-5 particle agglomerates in the as-synthesized form, grown from a stirred gel with SiO_2:Fe_2O_3-ratio $\simeq$ 90. XBB 887-7164

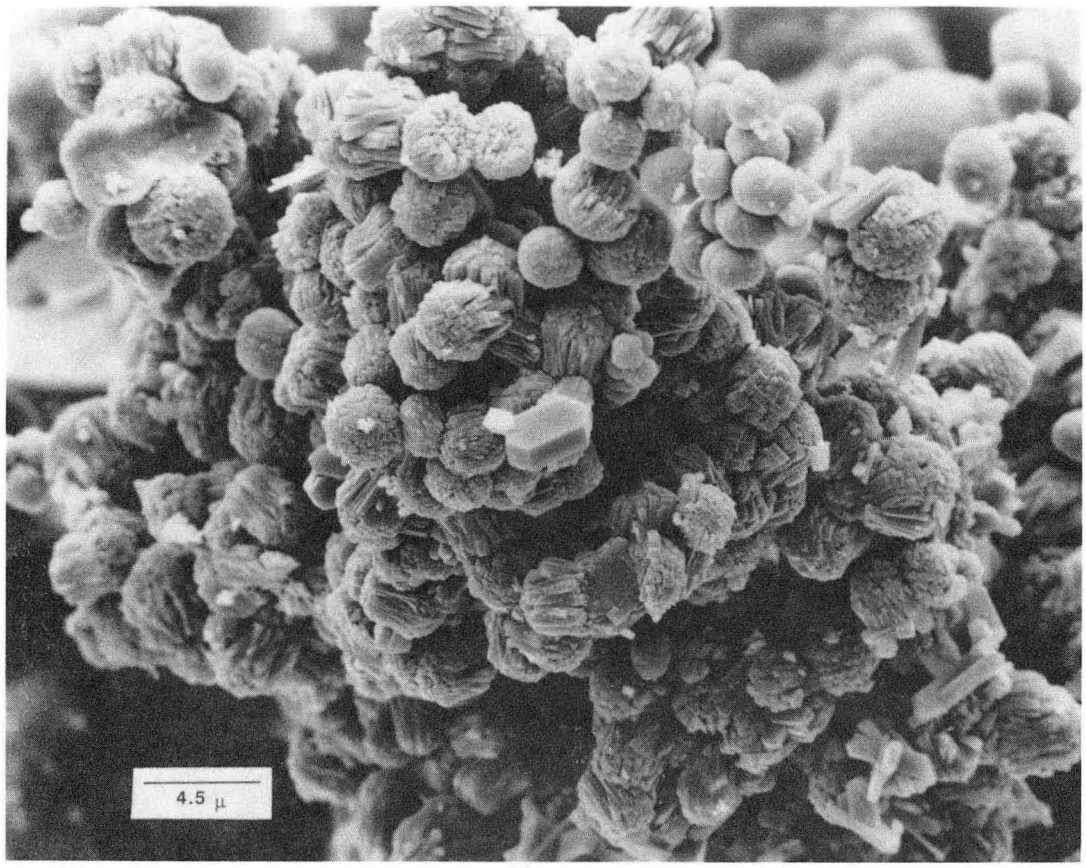

Figure 2.4 - SEM image of iron silicate molecular sieve in the as-synthesized form, grown from an unstirred gel with SiO_2:Fe_2O_3-ratio $\simeq$ 50 showing intergrown crystals and a prominant single crystal of FeZSM-5. XBB 8711-10114

2.3.2. Effects of added cations during crystallization

The effects of alkali cations (Li^+, Na^+ and K^+) on the size and morphology of FeZSM-5 are also investigated. Crystals of FeZSM-5 are grown in the presence of Li, Na and K nitrate salts in a manner analogous to that described for growth of large crystals of the aluminosilicate ZSM-5 [21]. Figure 2.5 shows FeZSM-5 particles grown from unstirred gels with SiO_2:Fe_2O_3-ratio = 50 and (a) without alkali cations, (b) with Li cations, (c) with Na cations and (d) with K cations. As in the case of the aluminosilicate ZSM-5, addition of alkali cations results in larger particles. However, in the iron silicates

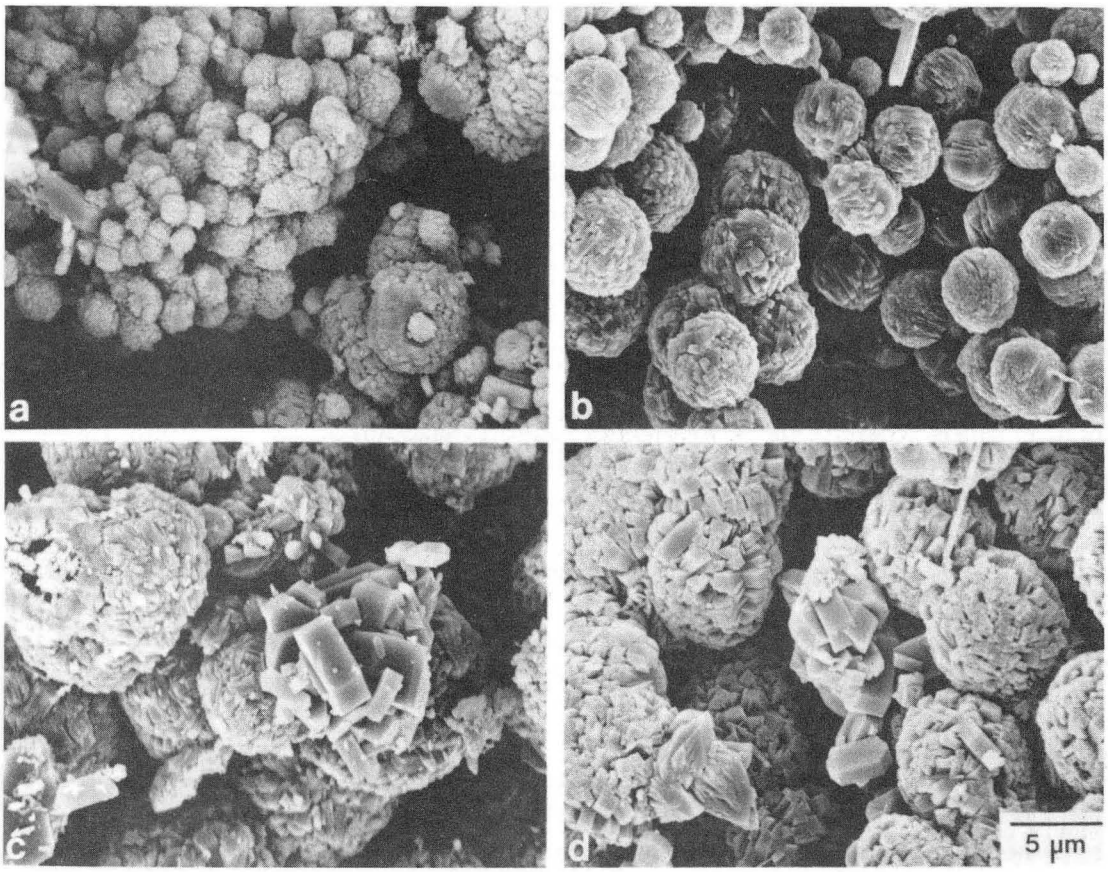

XBB 886-6206

Figure 2.5 - SEM images of iron silicate molecular sieves in the as-synthesized form, grown from unstirred gels with SiO_2:Fe_2O_3-ratio $\simeq$ 50, (a-)grown without additional alkali cations; (b)-grown with added Li cations; (c)-with Na cations; and (d)-with K cations.

only a few percent of the particles are large ($\geq$3 μm long) single crystals and most of the particles are agglomerates of smaller single or intergrown crystals. These agglomerates increase in size as the size of the added cation increases from Li^+ to K^+. Additionally the single crystals in the iron silicate samples are larger for the batches grown in the presence of sodium and potassium cations, whereas in the aluminosilicate case the largest single crystals were produced in the batches with lithium cations.

2.3.3. Effects of thermal and hydrothermal treatments

Scanning electron microscopy does not reveal any change in the size or the morphology of the FeZSM-5 particles after heat or steam treatments; also no second phase particles are observed in the calcined or steam treated samples.

2.4. Summary

Stirring the gel with a moderate to high iron concentration during crystal growth produces iron silicate particles with small, uniform size important for minimizing intracrystalline diffusion during catalytic processes. To understand the crystallization process, it is desirable to have large single crystals for electron microscopy or microprobe analysis. Large single crystals of FeZSM-5 are still elusive. Crystallization without agitation of the gel results in some small single crystals but predominantly large agglomerates of small crystallites are produced. Addition of alkali cations to the iron silicate gel during crystallization leads to a higher percentage of single, twinned and intergrown FeZSM-5 particles; however, most of the sample still consists of large particle agglomerates of small crystallites.

CHAPTER 3

IRON DISTRIBUTION IN FeZSM-5

It is important to know the distribution of iron in the FeZSM-5 particles before thermal and hydrothermal treatments since it will probably affect the distribution of the catalytically-active phase formed by the steam treatment.

3.1. Background: X-ray emission spectroscopy in the transmission electron microscope

Presented here is a brief introduction to x-ray emission spectroscopy, also called energy dispersive spectroscopy, in the TEM; for a more detailed description see references [22,23].

3.1.1. Generation and detection of the x-ray signal

Transmission electron microscopy (TEM) differs from scanning electron microscopy (described in chapter 2) in that the specimen cannot be a bulk sample but must be a very thin foil through which the electrons are transmitted. This technique gives through-thickness and not surface information about the specimen. In a TEM the electrons that have passed through the specimen are combined to form an image of the specimen using post-specimen lenses; this is described further in chapter 4.

High energy electrons can interact elastically or inelastically with a specimen. Inelastic collisions result in the emission of electrons and electromagnetic waves from the specimen (fig. 3.1) that can provide useful information about the material; e.g. SEM uses secondary or backscattered electrons to form topographic images of the specimen surface.

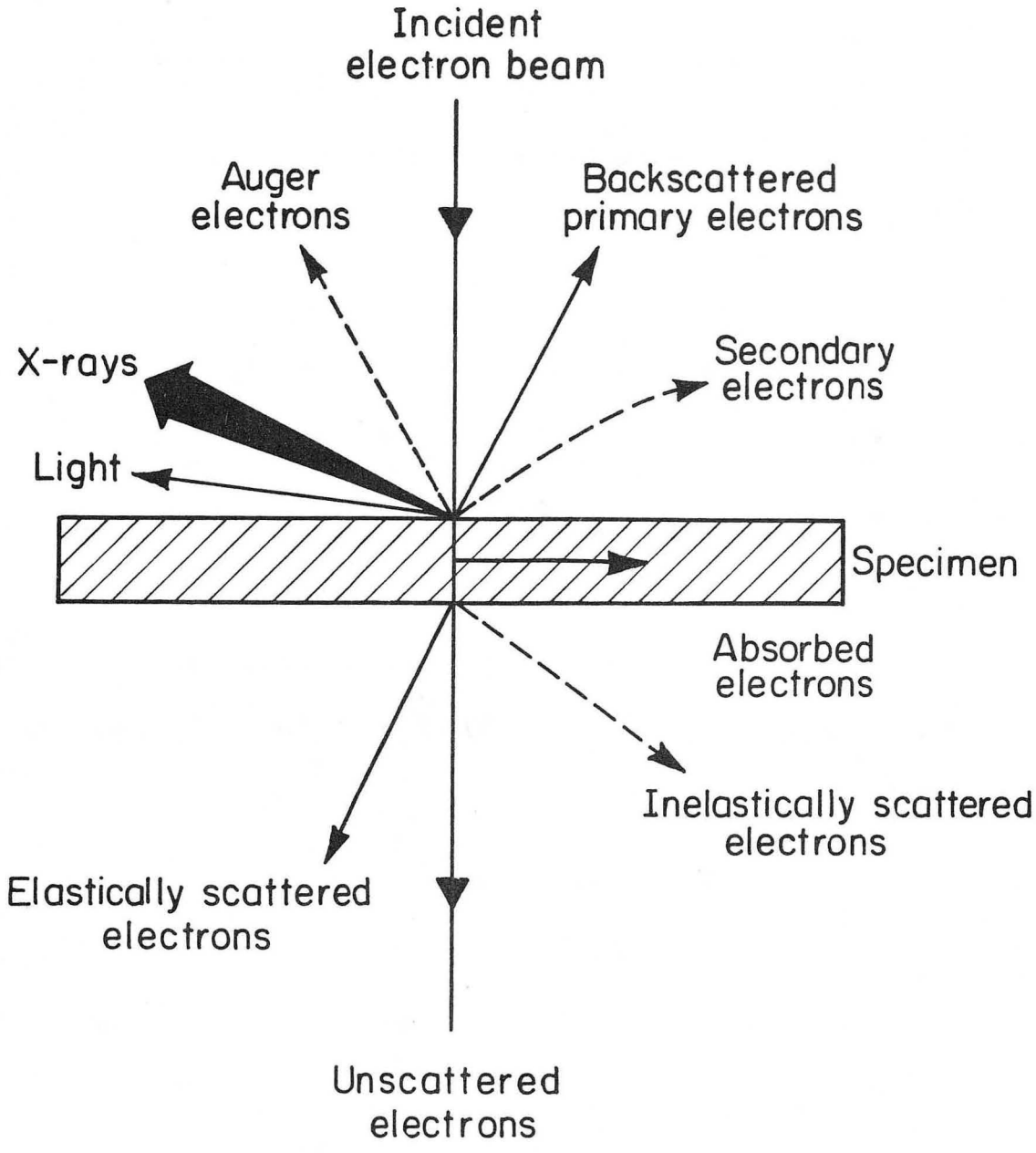

XBL 8010-6136

Figure 3.1 - The signals generated by the interaction of the high energy electron beam with a thin specimen.

Valuable composition information may obtained by collection and analysis of the x-ray spectrum emitted from the electron-probed specimen. If an x-ray spectrum is collected in a SEM the information is representative of a large area (1-2 μm) of the specimen due to electron beam spreading as it penetrates the bulk sample. In the case of a TEM since the

specimen is a thin foil of material, spreading of the electron beam is minimal and the characteristic x-ray data can be collected from an area smaller than 40 nm diameter (fig. 3.2).

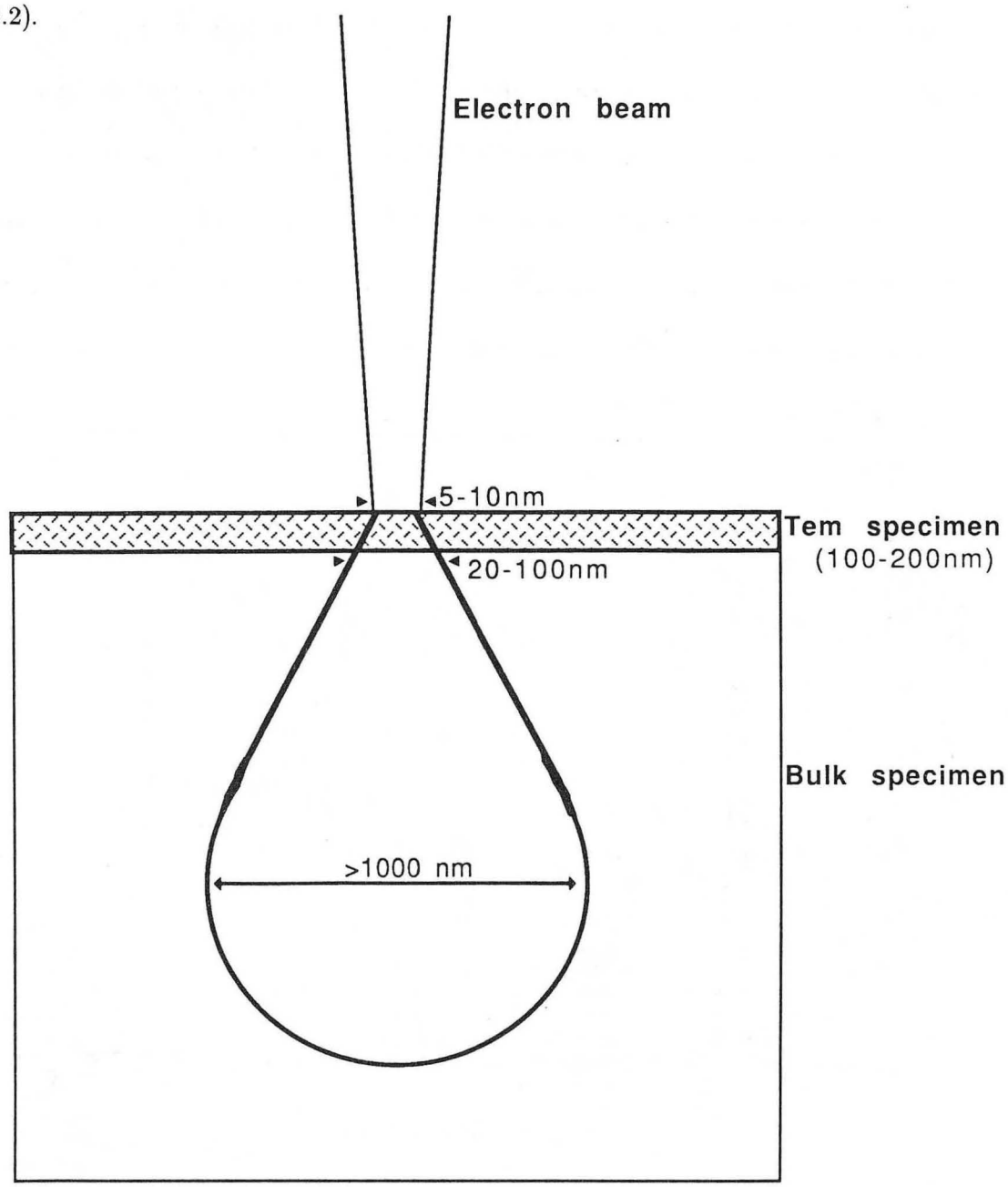

Figure 3.2 - The electron beam/specimen interaction volume comparing the spatial resolution of x-ray analysis in thin and bulk specimens.

In a TEM the characteristic X-rays are detected using an energy dispersive spectrometer (EDS). The X-ray photons pass through a protective beryllium window and strike a lithium-drifted silicon detector creating electron-hole pairs; this signal is amplified and then a multichannel analyzer discriminates the signal in terms of the incident x-ray energy. The output to a CRT is usually in the form of a spectrum of x-ray intensities versus energy. A typical x-ray spectrum is shown in figure 3.3. X-rays with energies less than 0.8 keV are not detected because they are absorbed in the beryllium window. Light elements can be detected with special windowless detectors or "thin-

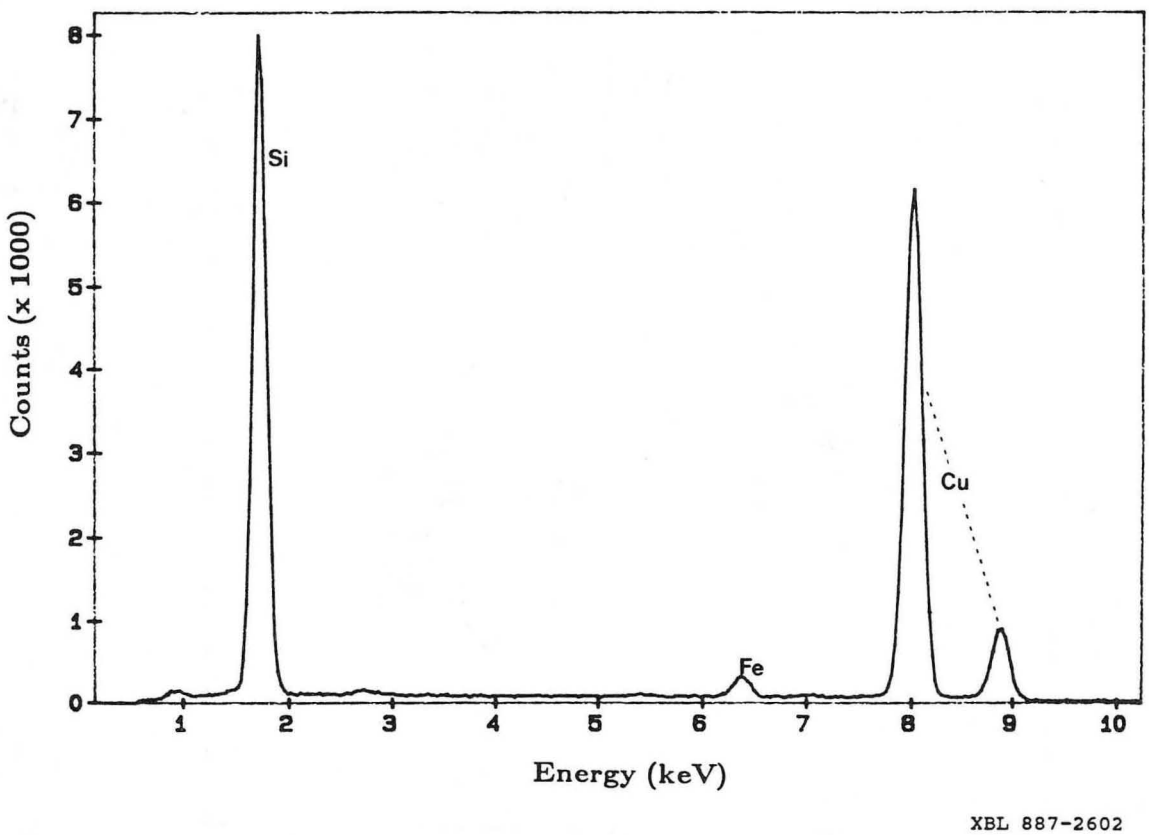

Figure 3.3 - An energy dispersive x-ray spectrum of FeZSM-5 with SiO_2:Fe_2O_3-ratio = 90, grown from a stirred gel. The silicon and iron peaks are from the FeZSM-5 particles, while the copper peaks are from the support grid.

window" detectors in which the window is typically a polymer, however these are expensive and are not generally used for routine analysis.

3.1.2. Quantification

Quantification of the x-ray spectrum is relatively straightforward using the equation

$$\frac{C_A}{C_B} = k_{AB} \frac{I_A}{I_B} \tag{3.1}$$

where C_A and C_B are the atomic (or weight) percents of elements A and B in the analyzed volume, I_A and I_B are the characteristic x-ray intensities above background for elements A and B, and k_{AB} is the appropriate experimentally determined proportionality constant. This ratio method assumes that the "thin foil criterion" is met, i.e., absorption and fluorescence of X-rays during their passage out of the specimen are negligible. In the case of zeolites, the thin foil criterion [24] is met for specimens prepared by ultramicrotomy, since the samples can easily be sliced less than 100 nm thick [25].

The background (bremsstrahlung) x-ray intensity is modeled using software provided by the minicomputer that is part of the EDS system. Generally in the energy region above 2keV a straight line fit to the background is sufficient, however in the 0.8-2keV region the background intensity changes rapidly and a more complex function is used in the modeling sequence.

Since for this work the only x-ray peaks of interest were the silicon and iron peaks, the background was only modeled and subtracted in the vicinity of these peaks and not over the entire spectrum (fig. 3.4). After subtraction of the background, the intensities in the silicon and iron peaks were determined. The intensities were taken to be the total number of x-ray counts in 0.40 keV windows, 1.54 to 1.94 and 6.20 to 6.60 keV for silicon and iron, respectively. These energy windows correspond to the silicon K_α and K_β peaks

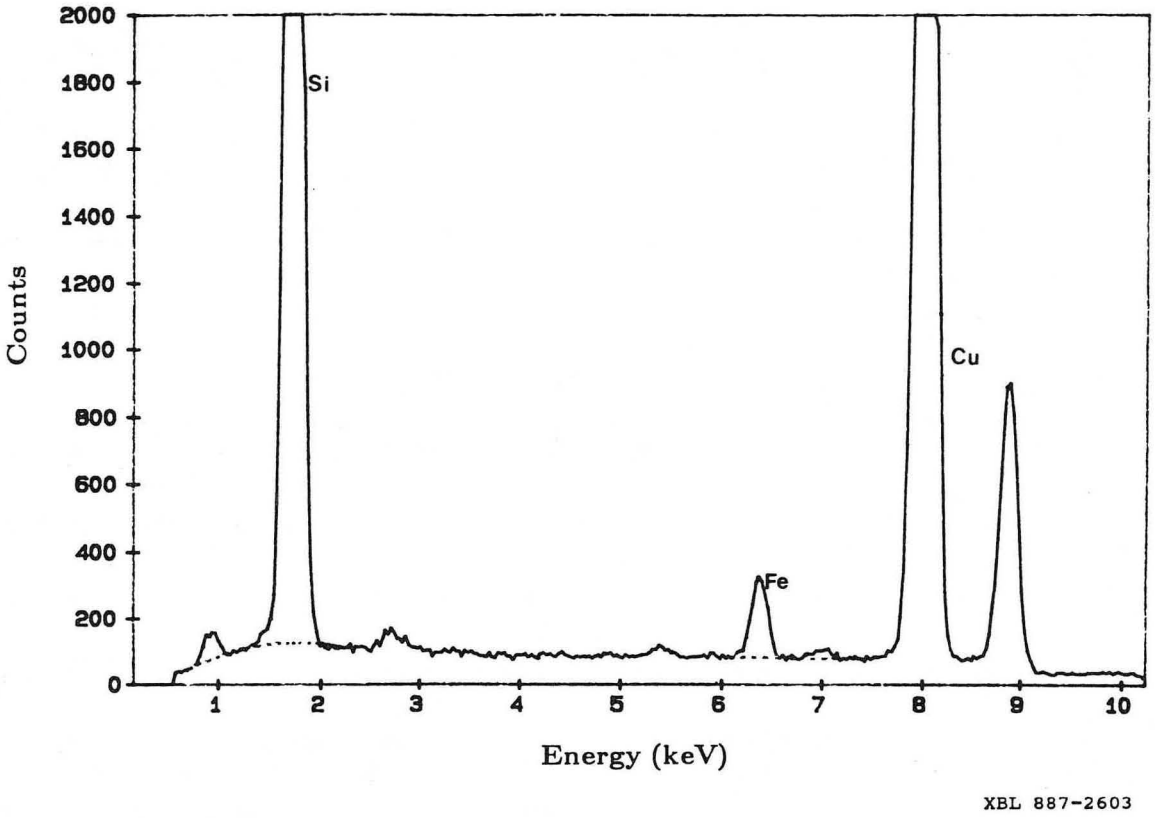

Figure 3.4 - The EDS spectrum from fig. 3.3 with expanded scale to show background model (dotted line) under the Si and Fe peaks.

and the iron K_α peak.

The proportionality constant, k_{SiFe}, was experimentally determined on an olivine standard (described in appendix B) prepared for TEM using ultramicrotomy. Over 30 spectra from different olivine particles were collected and analyzed to insure good statistics from a representative sample. The spectra were analyzed as described above and k_{SiFe} was determined to be 1.5 using equation 3.1 where C_{Si} and C_{Fe} are atomic percentages. This experimentally determined k-factor is only meaningful for an analysis performed in the energy intervals as described above and should not be compared with other k-factors determined for other energy windows.

3.2. Inter-particle study

The inter-particle iron distribution in the iron silicate molecular sieves has been studied using X-ray emission spectroscopy in the transmission electron microscope. The effects of gel iron concentration, stirring during crystallization, particle size, as well as thermal treatment were considered. For the purposes of this discussion, the word "particle" is used to describe the particle aggregates shown in figure 3.5, not to describe the individual crystallites making up the agglomerate.

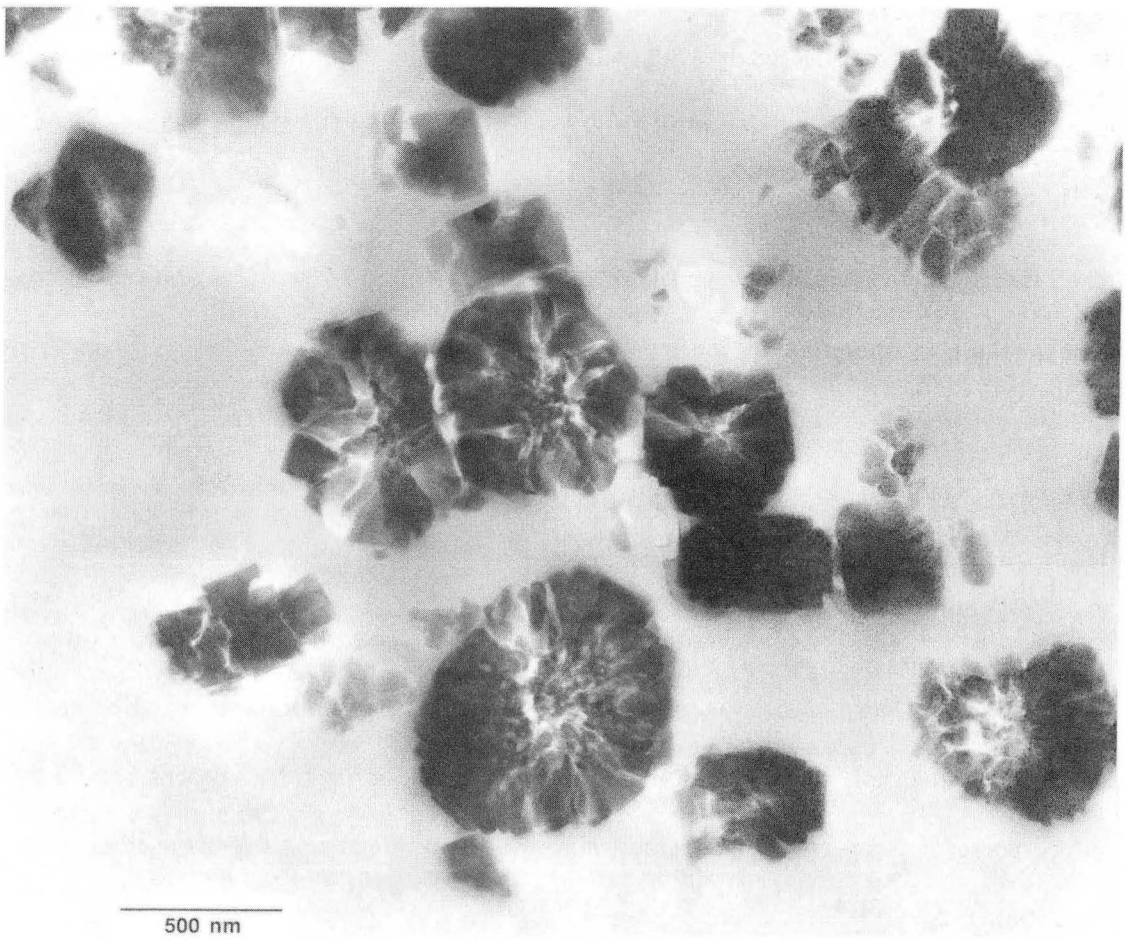

XBB 870-10116

Figure 3.5 - TEM image of microtomed thin section of as-synthesized FeZSM-5 particles, embedded in an acrylic resin. The iron silicate was grown from a stirred gel with SiO_2:Fe_2O_3-ratio = 200.

3.2.1. Procedures

The samples were in the as-synthesized and calcined forms grown from stirred and unstirred gels with SiO_2:Fe_2O_3-ratios $\simeq$ 50, 90 and 200. TEM specimens consisted of uniformly thin (90-100nm) sections of the iron silicate particles embedded in an acrylic resin (fig. 3.5); they were prepared by ultramicrotomy, described in detail elsewhere [26, 27] Experiments were carried out in a Phillips 400T TEM/STEM operated at 100kV accelerating voltage. X-rays were detected with a Kevex, beryllium-window, X-ray detector; spectra were collected for 300 seconds (livetime) to minimize statistical counting uncertainty. Probes were formed, as best possible, to equal the size of the particle probed without illuminating adjacent particles.

Energy dispersive X-ray spectra (EDS) of all FeZSM-5 samples showed silicon and iron peaks corresponding to the iron silicate molecular sieve particles, and copper peaks resulting from the copper support grids (fig. 3.3). In some spectra, a small chromium peak was observed; this was probably due to a small amount of chromium contamination from the stainless steel crystallization vessel.

On average, 20 spectra from various particles were collected for each sample; this was to insure that the spectra were representative of the bulk samples. For each spectrum, quantification was carried out as described in section 3.1.2. Absorption and fluorescence corrections were not necessary since the specimens met the thin-film conditions ($<$150nm) [24].

3.2.2. Results and discussion

Figure 3.6 is a histogram of the results for the stirred and unstirred as-synthesized samples with SiO_2:Fe_2O_3-ratio $\simeq$ 50. The measured mean value of Si/Fe for both sam-

ples is 25. The histogram shows that the stirred sample has a more homogeneous particle-to-particle iron distribution with all of the analyzed particles having a Si/Fe-ratio between 21 and 31 and most are between 21 and 26. This is in contrast to the unstirred sample with its Si/Fe-ratio ranging from 16 to 41.

The homogenizing effect of stirring the gel during crystallization is shown more dramatically in figure 3.7 for the samples with SiO_2:Fe_2O_3-ratios $\simeq$ 90, where the spread in the data for the unstirred sample is four times that of the stirred sample.

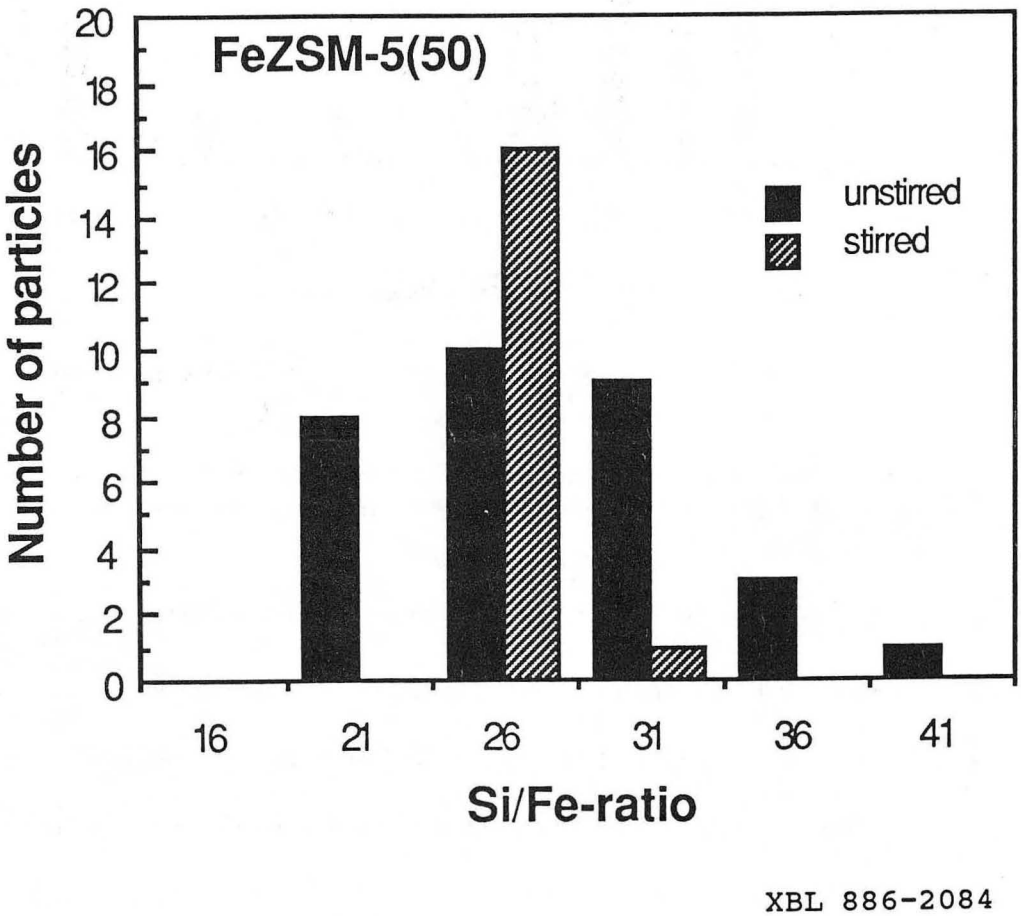

Figure 3.6 - Histogram of experimentally determined Si/Fe-ratios for as-synthesized FeZSM-5 particles grown from stirred and unstirred gels with SiO_2:Fe_2O_3-ratio $\simeq$ 50.

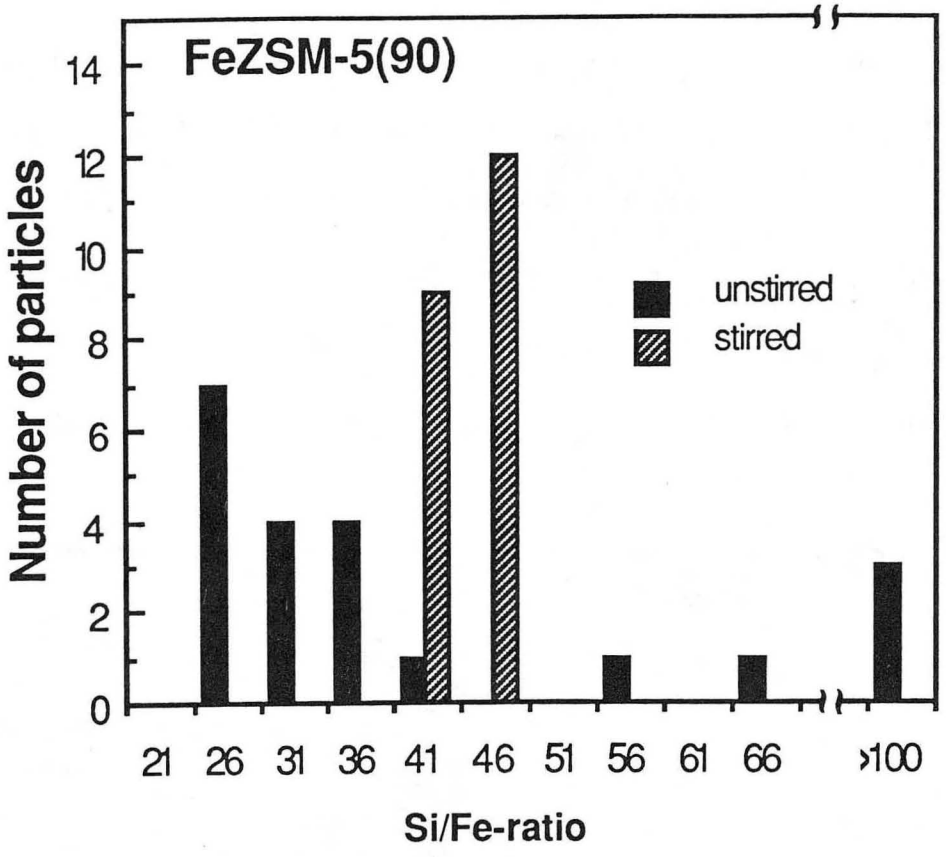

Figure 3.7 - Histogram of experimentally determined Si/Fe-ratios for as-synthesized FeZSM-5 particles grown from stirred and unstirred gels with SiO_2:Fe_2O_3-ratio $\simeq$ 90.

In the case of samples with SiO_2:Fe_2O_3-ratio $\simeq$ 200, stirring produces particles whose Si/Fe-ratios form a gaussian distribution between 56 and 111 with a mean value of 78 (fig. 3.8). At this very low level of iron (one iron atom per unit cell of ZSM-5) stirring improves but does not ensure homogeneity of the iron distribution amongst the particles. Collectively particles grown without stirring have the expected value of Si/Fe-ratio of 100, but individually these particles vary widely in iron content from the iron-rich with Si/Fe-ratio = 26 to the very silica-rich with measured Si/Fe-ratios up to 300.

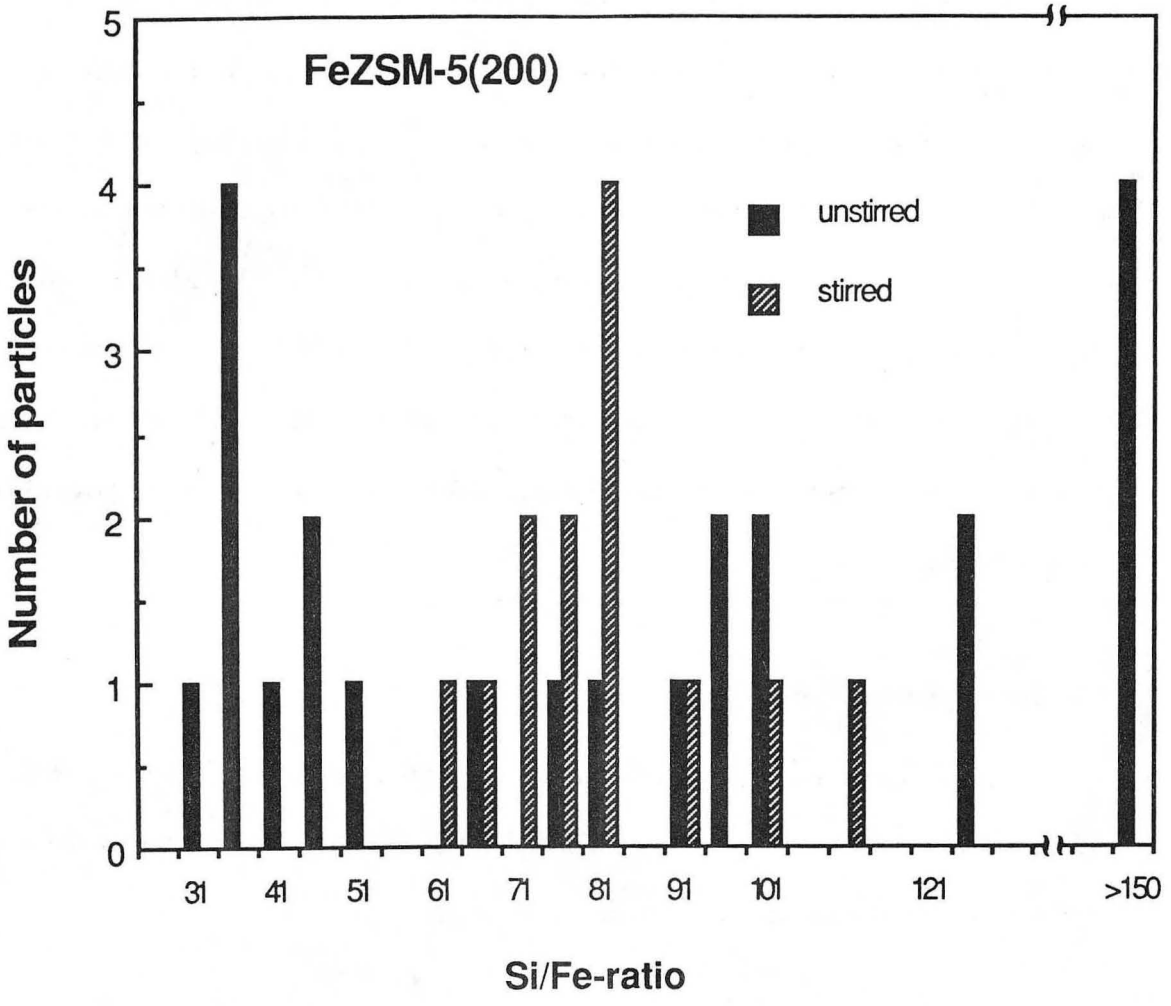

Figure 3.8 - Histogram of experimentally determined Si/Fe-ratios for as-synthesized FeZSM-5 particles grown from stirred and unstirred gels with SiO_2:Fe_2O_3-ratio $\simeq$ 200.

The effect of particle size on the distribution of iron amongst the FeZSM-5 particles can be seen best by comparing the mean Si/Fe-ratios for stirred and unstirred samples. As stated in chapter 2, the particle sizes of the stirred samples are 1 μm or less, while in the unstirred samples, particle diameters are greater than 1 μm. Although the iron content of the particles from the unstirred samples varies from one to another, the mean Si/Fe-ratios measured by XES for the unstirred samples of FeZSM-5 are comparable with those of the stirred samples. No correlation between size and iron content is observed.

The average Si/Fe-ratio is unchanged by thermal treatment for both stirred and unstirred samples. The particle-to-particle variations are the same for the unstirred samples before and after heat treatment, however the stirred samples show larger variations in the calcined forms at all three iron concentrations, suggesting that there is probably some iron migration occurring during thermal treatment [28]. This effect is most pronounced in the high silica sample where the iron might be able to migrate more easily to the particle surfaces during heat treatment. In samples with higher iron concentrations, a second iron oxide phase may form inside the ZSM-5 particles and reduce the migration of the iron to the outside of the particle.

3.3. Intra-particle study

This is an investigation of the distribution of iron amongst the FeZSM-5 particles on a finer scale, namely within selective regions of the particles and finally within the individual crystallites making up the particles.

3.3.1. Procedures

The iron distribution within the particles was studied on the as-synthesized FeZSM-5 samples grown in stirred and unstirred gels with SiO_2:Fe_2O_3-ratios $\simeq$ 50, 90 and 200. Specimens were prepared by microtomy and analyzed in a Philips 400T TEM/STEM as described in section 3.2.1. The electron probe was used to irradiate only a small portion of the FeZSM-5 particle at a time, thereby restricting the area from which the X-rays were generated.

Individual crystallites of the particles were investigated for iron segregation using a Vacuum Generators HB-501 STEM with a field emission gun equipped Link Analytical

windowless x-ray detector. The field emission gun is a very small source of electrons with very high brightness allowing the collection of an x-ray spectrum from a very small area of the specimen. Line profiles of individual FeZSM-5 crystallites were attained by scanning across the particle with a 1.8 nm (full width at tenth maximum) electron probe while the Link Analytical detector and computer system collected and stored the number of x-ray counts in each of eight preselected energy windows for each point probed. By comparing the line profile of silicon versus that of iron the distribution of iron throughout the individual crystallite may be determined qualitatively if not quantitatively.

3.3.2. Results and discussion

As shown in section 3.2 the iron content varies from particle-to-particle in the iron silicate FeZSM-5 grown from unstirred gels. Variations are also evident on the intra-particle scale; figure 3.9 shows the measured Si/Fe-ratios for different areas of the particle and for the particle thin section as a whole. The center is iron-rich with Si/Fe-ratio $\simeq 33$ while the outer edges are silicon-rich with measured Si/Fe-ratios between 124 and 151; these areas together give the particle thin section its overall Si/Fe-ratio of 70. In other words, although this particle on average has 1.4 iron atoms per ZSM-5 unit cell, the center actually has four times the concentration of iron as do the outer areas of the particle. If there is not significant migration of iron during thermal or subsequent hydrothermal treatment this distribution of the iron could result in the center of the particle being much more catalytically active then the outer edges; in some selective applications this might be desirable but in most reactions it is probably not an advantage. Accompanying the difference in iron concentration from the inside to the outside of a particle is a morphological change: internal crystallites are small, irregularly shaped and iron enriched while the larger crystals near the particle edges are silicon-rich and more crystallographic

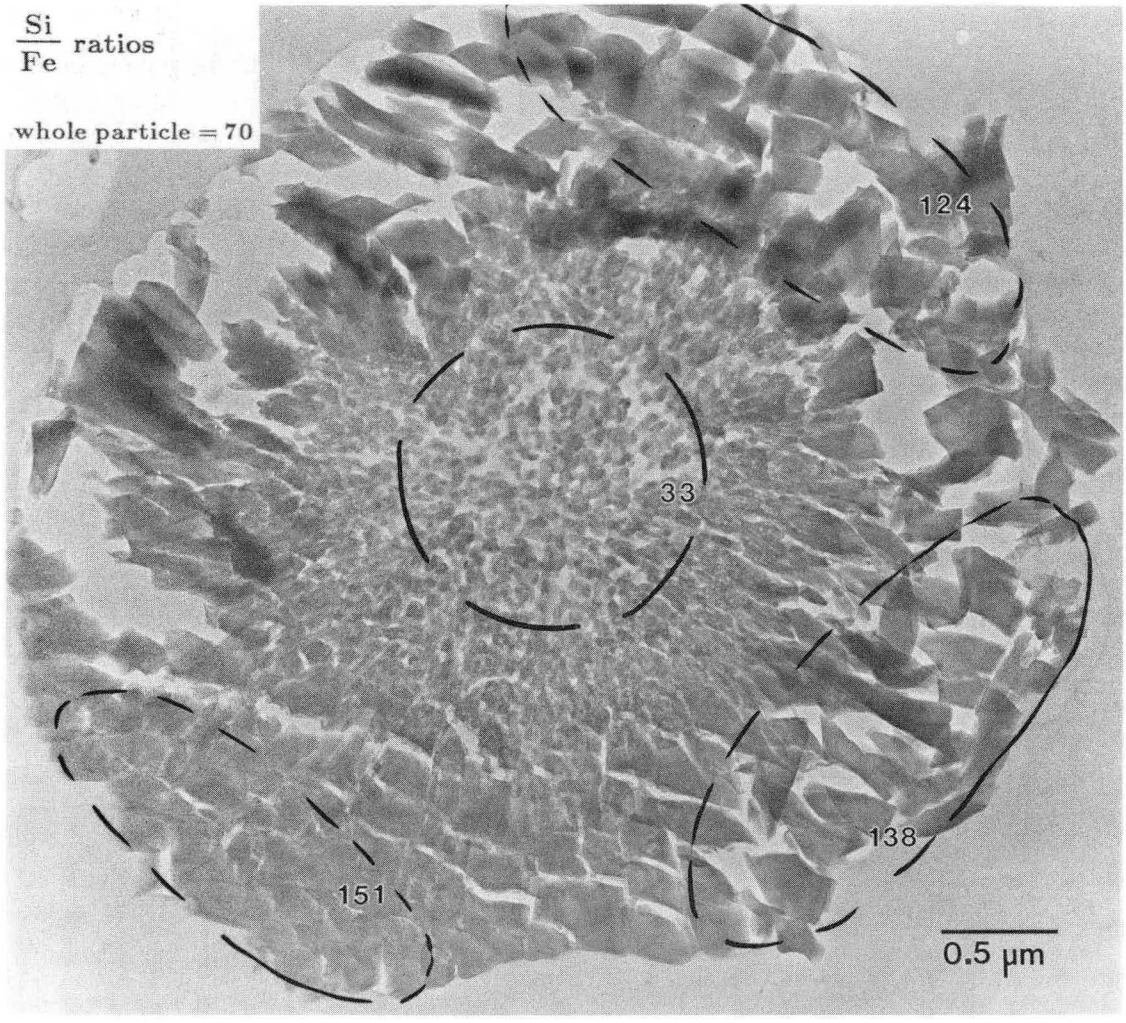

XBB 887-6972

Figure 3.9 - TEM image of a microtomed section of as-synthesized FeZSM-5 particle grown from an unstirred gel with SiO_2:Fe_2O_3-ratio $\simeq$ 200 showing Si/Fe-ratios measured in areas probed for determination of iron distribution.

in shape.

This relationship between morphology and iron content of the crystallite is observed in all unstirred samples even those grown from gels with high iron concentrations (fig. 3.10). The connection between iron concentration and morphology (and not necessarily the location within particle) is clearly illustrated in this figure where some of the small crystallites close to the edge of the particle are iron-rich and all large crystals probed are

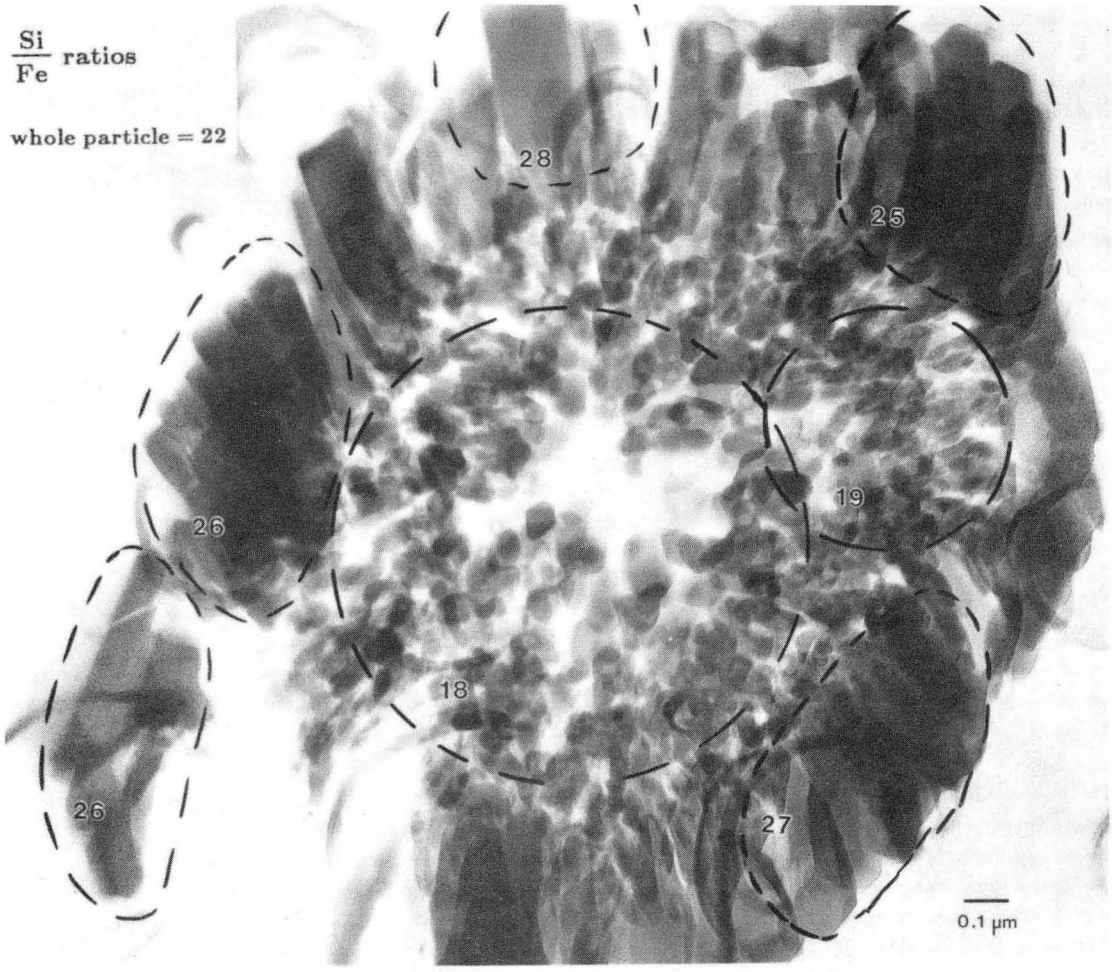

XBB 884-4154

Figure 3.10 - TEM image of a thin section of as-synthesized FeZSM-5 particle grown from an unstirred gel with SiO_2:Fe_2O_3-ratio $\simeq$ 50 showing Si/Fe-ratios for different areas of the particle.

found to be relatively iron poor. In this high iron content particle the iron segregation results in regions of the particle containing about 5.5 iron atoms per unit cell and other regions with four iron atoms per unit cell. This inhomogeneity in the iron distribution probably is not as significant to the catalytic activity or selectivity as the four fold difference found in the sample with very low iron concentration.

The distribution of iron throughout the unstirred as-synthesized particles suggests that the FeZSM-5 particles nucleate in the iron-rich gel and grow in a then iron-depleted

gel. As demonstrated by comparison of SEM images and the inter-particle iron distributions of particles grown from stirred and unstirred gels, agitation promotes nucleation and it prevents strong concentration gradients from developing, additionally if the agitation is vigorous enough, particles grown from stirred gels should have a homogeneous intra-particle iron distribution.

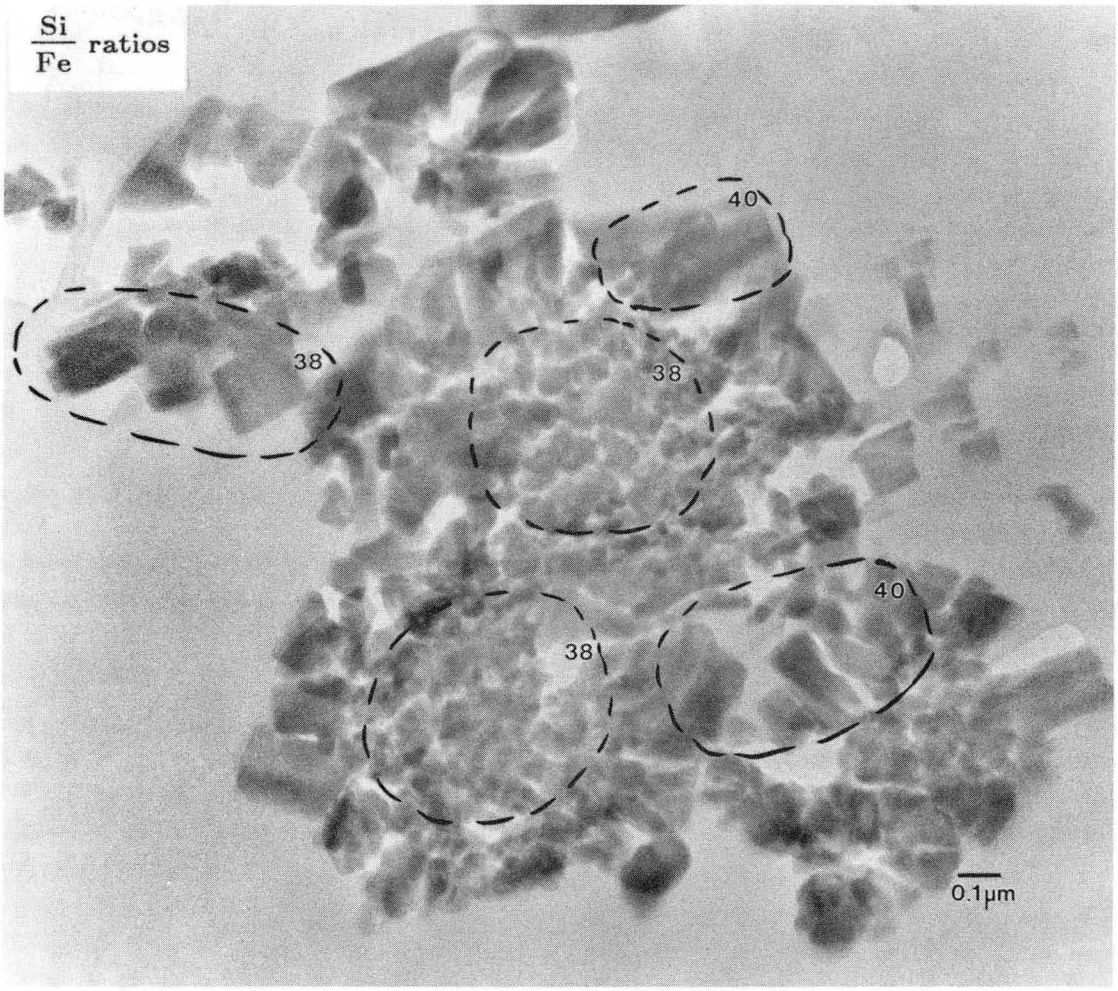

XBB 887-6975

Figure 3.11 - TEM image of a microtomed section of as-synthesized FeZSM-5 particles grown from a stirred gel with SiO_2:Fe_2O_3-ratio $\simeq$ 90 showing Si/Fe-ratios measured in areas probed for determination of iron distribution.

Particles grown from stirred gels with moderate to high iron concentrations (SiO_2:Fe_2O_3-ratios $\simeq$ 90 to 50) typically have uniform iron distributions throughout the particles. As can be seen in figure 3.11 the iron concentration is constant; whether the area probed is at the center or near the edge of the particle, or if the area consists of irregularly shaped crystallites or regular rectangular or cuboidal shapes, the iron concentration is always about 2.5 iron atoms per unit cell ZSM-5.

At the very low level of iron (one iron atom per unit cell of ZSM-5) stirring could not ensure an even distribution of iron from one particle to another and also on the intra-particle scale homogeneity can not be maintained at the standard rate of stirring the gel in the autoclave. Figure 3.12 shows a typical particle section from the lowest iron sample. The center of the particle contains approximately two irons per unit cell ZSM-5 but the edges contain only about one per unit cell. Compared to the particles grown from unstirred gel with the same SiO_2:Fe_2O_3-ratio $\simeq$ 200 (fig. 3.9) stirring has improved the homogeneity of the iron in the particle quite significantly, but the relationship between morphology of the individual crystallites and the iron segregation is still apparent. Whenever there is an inhomogeneous distribution of iron in a given particle the regions that are higher in iron are made up of small irregular crystallites and areas of low iron concentration are made up of larger more well defined crystals.

Individual FeZSM-5 crystallites were line profiled to determine the applicable scale of the hypothesis that the particles grown from unstirred gels nucleate in the iron-rich regions of the gel and continue their growth in an iron depleted gel [29]. Figure 3.13 shows the silicon and iron profiles typical of the individual crystallites composing the FeZSM-5 particles grown from unstirred gels with SiO_2:Fe_2O_3-ratio $\simeq$ 50; the crystallite boundaries are marked by the silicon line profile's sharp rise and fall in intensity. By

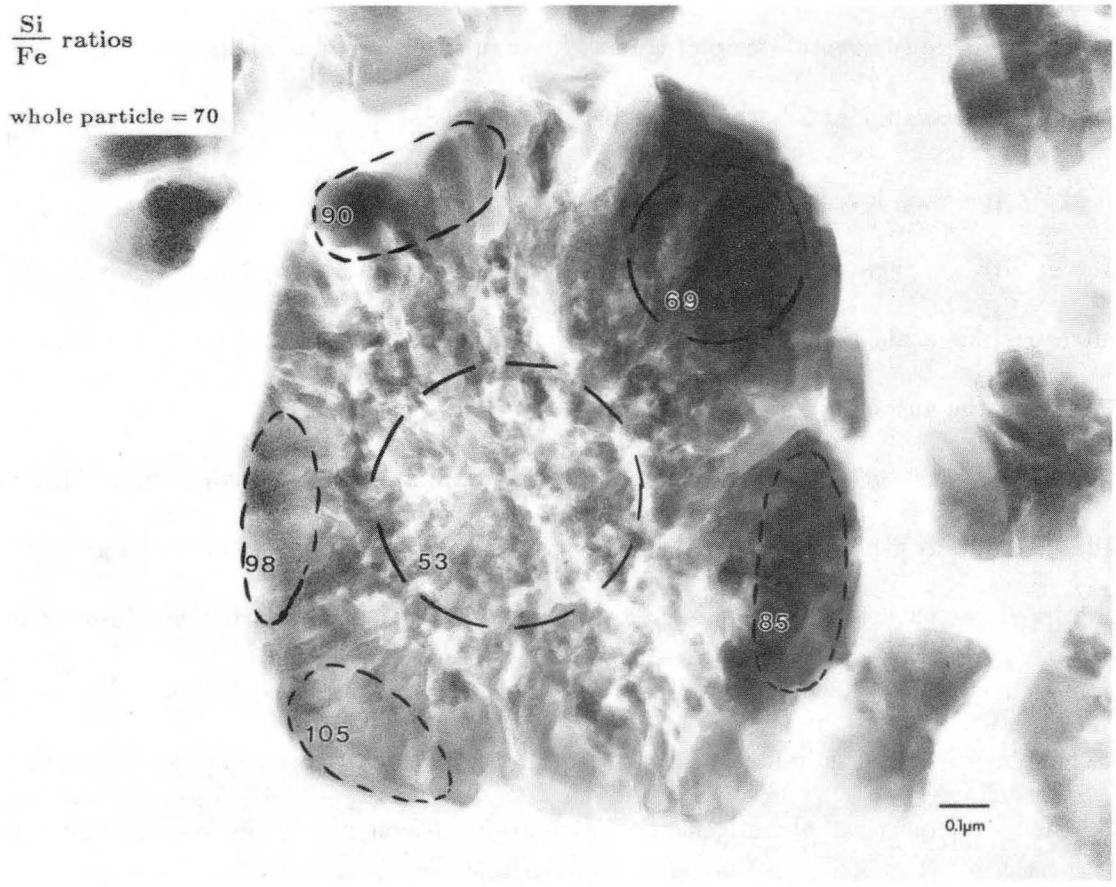

XBB 886-6203

Figure 3.12 - TEM image of a microtomed section of as-synthesized FeZSM-5 particle grown from a stirred gel with SiO_2:Fe_2O_3-ratio $\simeq$ 200 showing Si/Fe-ratios and areas probed.

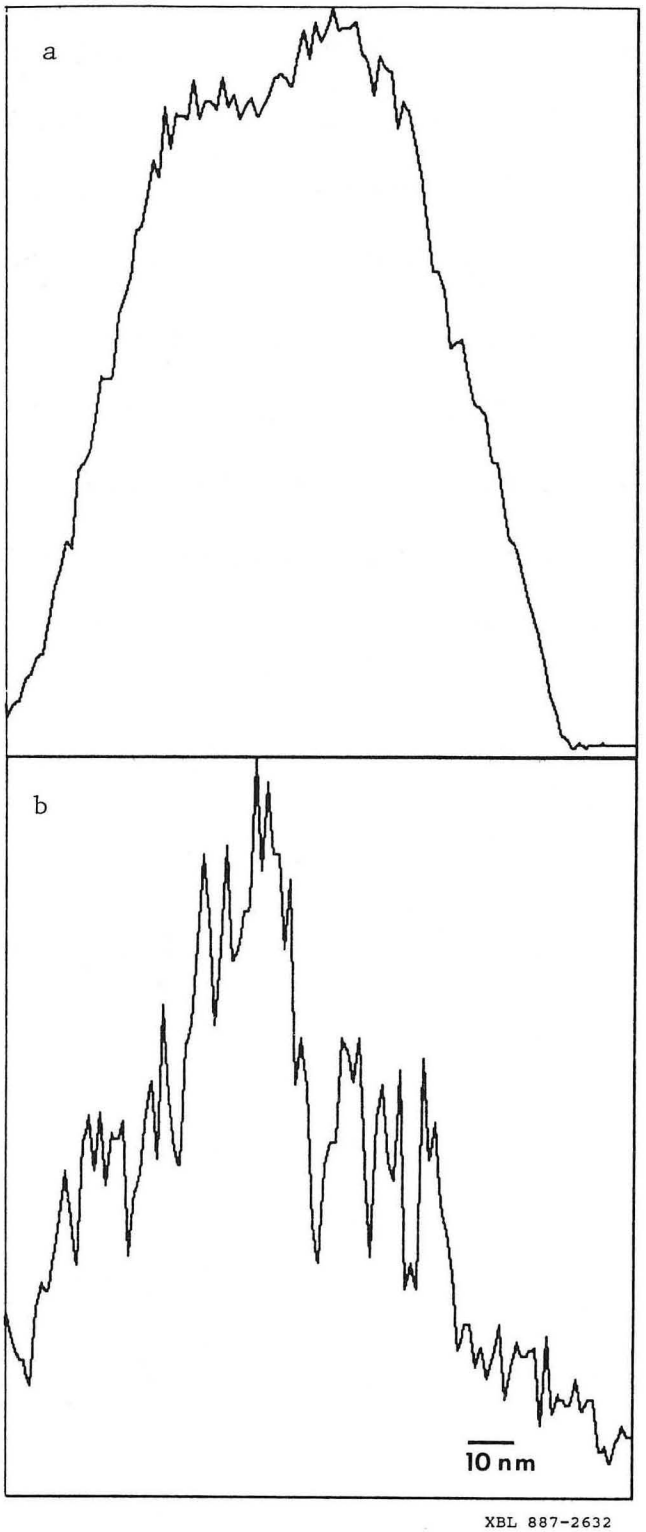

Figure 3.13 - Typical silicon (a) and iron (b) line profiles from a single FeZSM-5 crystallite in an as-synthesized particle grown from an unstirred gel with SiO_2:Fe_2O_3-ratio $\simeq$ 50.

comparing the iron profile with that of the silicon it is observed that the iron content is greater in the middle of the crystal and lower near its edges. This is observed for all of the crystallites of a particle, both those that are small irregular and iron-rich and those that are larger and regularly shaped; thus the iron-rich nucleation with growth in an iron depleted gel hypothesis is confirmed on the intra-crystal scale.

The x-ray line profiling of the individual crystallites of the FeZSM-5 particles grown from stirred gels with SiO_2:Fe_2O_3-ratio $\simeq$ 50 shows them to have very constant iron content from edge to edge (fig. 3.14). This distribution is observed for all of the crystallites regardless of shape or size.

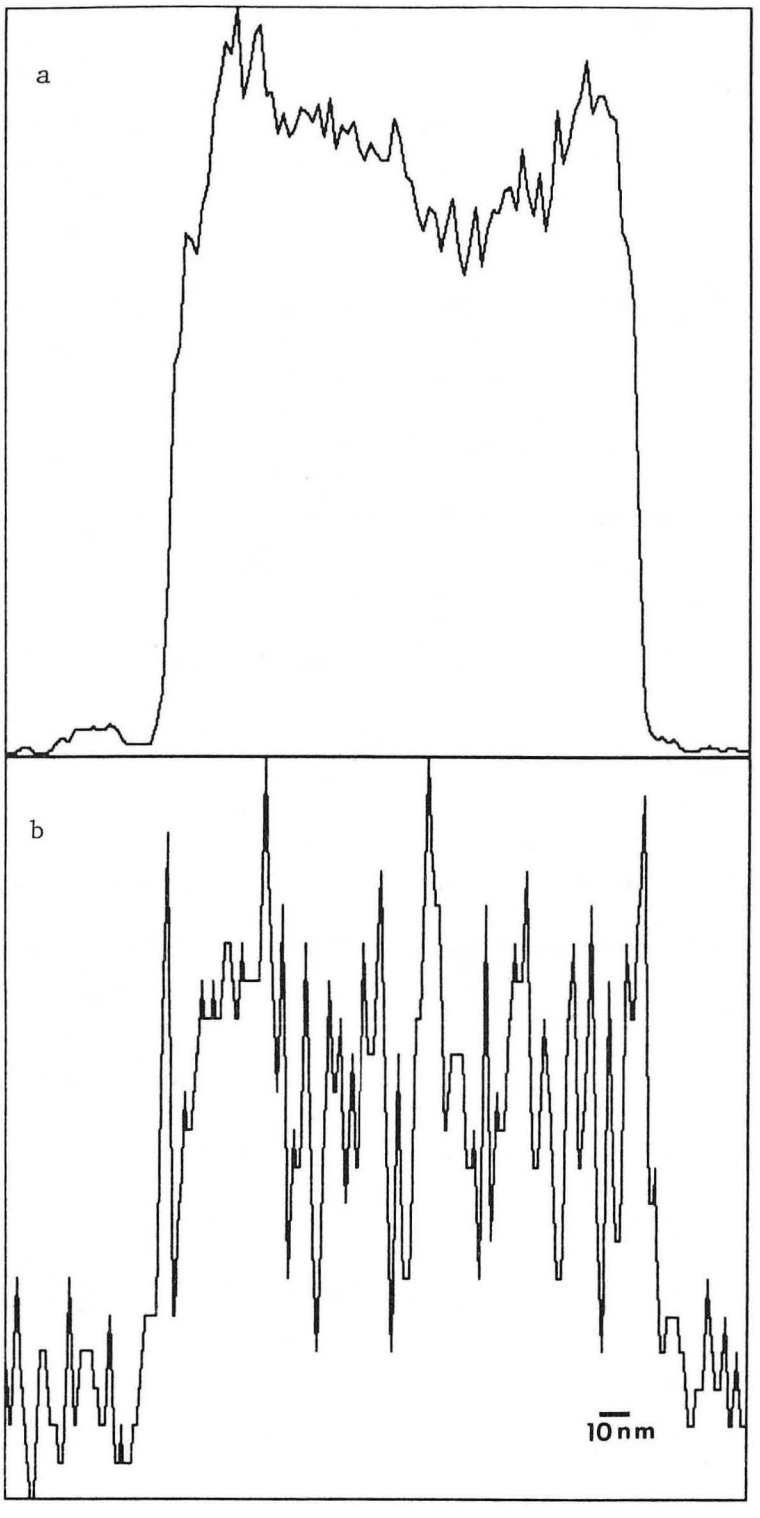

Figure 3.14 - Typical silicon (a) and iron (b) line profiles from a single FeZSM-5 crystallite in an as-synthesized particle grown from a stirred gel with SiO_2:Fe_2O_3-ratio $\simeq$ 50.

3.4. Summary

X-ray emission spectroscopy performed in the transmission electron microscope has shown that the Si/Fe-ratio of the as-synthesized FeZSM-5 particles is independent of particle size and stirring, although the homogeneity of the inter-particle iron distribution does improve with stirring. As expected, thermal treatments do not significantly change the average Si/Fe-ratios of the FeZSM-5; however, the particle-to- particle variations do increase in samples grown from stirred gels, particularly in very low iron materials.

Stirring has a profound effect on the iron distribution within the FeZSM-5 particles and within their constituent crystallites. Particles grown from unstirred gels are made up of two distinct kinds of crystallites: those usually in the center of the particle are small, irregularly shaped and high in iron, and those near the edges have much lower iron content but are larger and regular shapes. This indicates that these particles nucleate in an iron-rich gel and continue their growth in an iron-depleted gel. This relationship between crystallite morphology and its iron content was also observed in the particles grown from stirred gels with very low iron content, and was probably a result of insufficient stirring to maintain homogeneity of the small iron content within the gel. Particles grown from stirred gels with moderate to high iron concentrations were found to be homogeneous on all spatial scales: inter-particle, intra-particle and intra-crystallite.

CHAPTER 4

MICROSTRUCTURE OF FeZSM-5

Transmission electron microscopy (TEM) techniques, conventional bright field imaging, selected area diffraction, high resolution imaging and microdiffraction, are used to study the microstructure of FeZSM-5 as a function of synthesis and processing conditions.

4.1. Background: Transmission electron microscopy

This description of some of the various imaging and diffraction modes possible in the transmission electron microscope (TEM) is meant to provide a basic intuitive understanding to those unfamiliar with such techniques. For a more in-depth qualitative description or a rigorous mathematical description of the techniques the reader is referred to several excellent texts [22, 23, 30 - 33].

As mentioned in chapter 3, in transmission electron microscopy electrons pass through a specimen and yield information about the internal structure of the sample. Transmission electron microscopes consist of an electron source, an area for holding and manipulating the sample and several electromagnetic lenses. Pre-specimen lenses focus the electron beam onto the specimen while post-specimen lenses provide image magnification. The most important part of any TEM is the objective lens which serves two essential functions (fig. 4.1). One is to bring all electrons scattered through the same angle from different areas of the specimen to a point of focus at its back focal plane. This intensity distribution is a map of electron scattering angles from the specimen called the diffraction pattern. The second, often more important, function of the lens is to form an image of the specimen. This occurs when electrons scattered from individual points of the

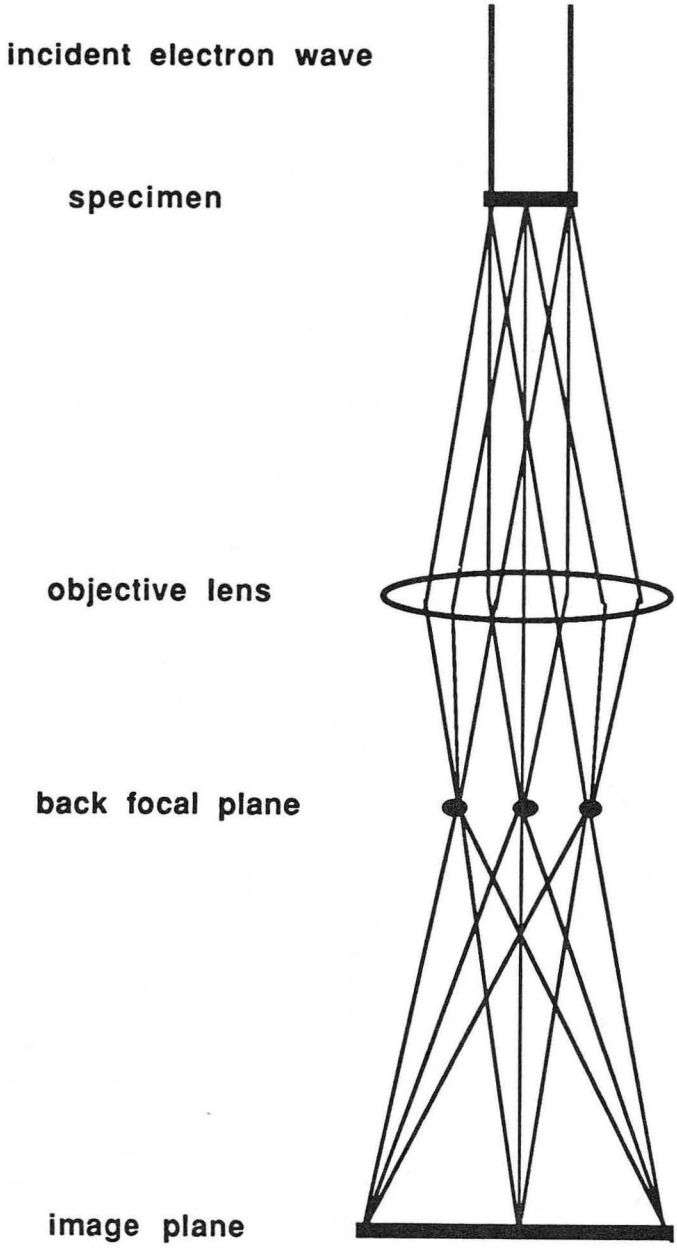

XBL 889-3155

Figure 4.1 - Schematic diagram of geometry of the specimen and objective lens showing the diffraction pattern at the back focal plane and the image of the specimen at the image plane of the objective lens.

specimen are brought to the proper corresponding points in the image.

An amplitude contrast bright field image results when an aperture is inserted at the back focal plane of the objective lens to block all diffracted beams except the forward diffracted (transmitted) beam. Areas of the specimen that elastically or inelastically

scatter strongly decrease the amplitude of the transmitted beam and produce darker areas in the image and parts of the specimen that only interact weakly appear bright in the image. Analogously, dark field images are formed using electrons that have been scattered away from the transmitted beam by the specimen, yielding images of opposite contrast. Amplitude contrast images are particularly useful for determining the extent and location of various phases in the sample.

High resolution electron microscopy uses many diffracted waves in conjunction with the transmitted wave to form an image; the amplitudes and the phases of the waves are combined coherently to give contrast due to constructive and destructive interferences. For a thin specimen under well-defined focus conditions, the atomic arrangement of scattering species may be resolved in the image [34].

Electron diffraction patterns from specific areas of the specimen are obtained by using an aperture at the image plane of the objective lens to limit the area contributing to the diffraction pattern. Due to spherical aberration and possible incorrect focusing of the objective lens, the area contributing to the selected area diffraction pattern can only be limited to about 1 μm with this selected area diffraction technique. In order to obtain a diffraction pattern from smaller areas a technique called microdiffraction is used. In this case, the condenser lens system is used to form a small (1-50 nm) probe of electrons, with a restricted range of incident angles, onto the specimen. No aperture is used at the objective lens image plane because only the illuminated area contributes to the diffraction pattern.

4.2. Experimental aspects

Both the bright field imaging and the high resolution imaging were performed in a JEOL 200CX microscope equipped with a high resolution objective lens, operating at its

maximum accelerating voltage 200 kV. At the expense of image contrast, maximum accelerating voltage was used to minimize the electron beam induced damage of the zeolite structure by minimization of its ionization cross-section [35- 39].

Microdiffraction was performed on an analytical version of the JEOL 200CX operated at 200 kV in micro-microdiffraction mode using a 20 nm probe. To prevent specimen contamination under the intense probe [22], the specimen was cooled to liquid nitrogen temperature in a GATAN cold stage.

As-synthesized, calcined and steam-treated samples of FeZSM-5 grown from stirred and unstirred gels with SiO_2:Fe_2O_3-ratios $\simeq$ 50, 90 and 200 were studied. The specimens consisted of uniformly thin (50-80 nm) sections of the iron silicate particles embedded in an acrylic resin (fig. 3.5) and were prepared by ultramicrotomy, described in detail elsewhere [26, 27].

4.3. Results and discussion

4.3.1. Conventional TEM imaging

As mentioned in the previous chapters, the cuboidal or spherical FeZSM-5 particles are actually aggregates of smaller FeZSM-5 crystallites. These crystallites have a bimodal size distribution (figs. 3.5, 3.9 - 3.12) many are 50-100 nm in diameter and others are 100-200 nm wide and up to 500 nm long. When FeZSM-5 is grown from unstirred gels, the particles form with the small crystals in the center surrounded by the larger crystals; in the case of stirred gels the crystallites are randomly arranged in the particle agglomerates without organization by shape or size. In and amongst these FeZSM-5 particles, no second phase material is detectable in either SEM or TEM images of the as-synthesized forms grown from stirred or unstirred gels.

Second phase particles ($\leq$ 2.5 nm) are detected after thermal treatment of samples with SiO_2:Fe_2O_3-ratio $\simeq$ 50 and in all FeZSM-5 samples after steam treatment at 550 °C for 2 hours. In the calcined FeZSM-5 grown from stirred gel with high iron content, the second phase particles are observed along the outer edges of the particles (fig. 4.2); in corresponding calcined sample grown from an unstirred gel the second phase particles are found on edges of the crystallites in the middle of the FeZSM-5 particles and seldom near

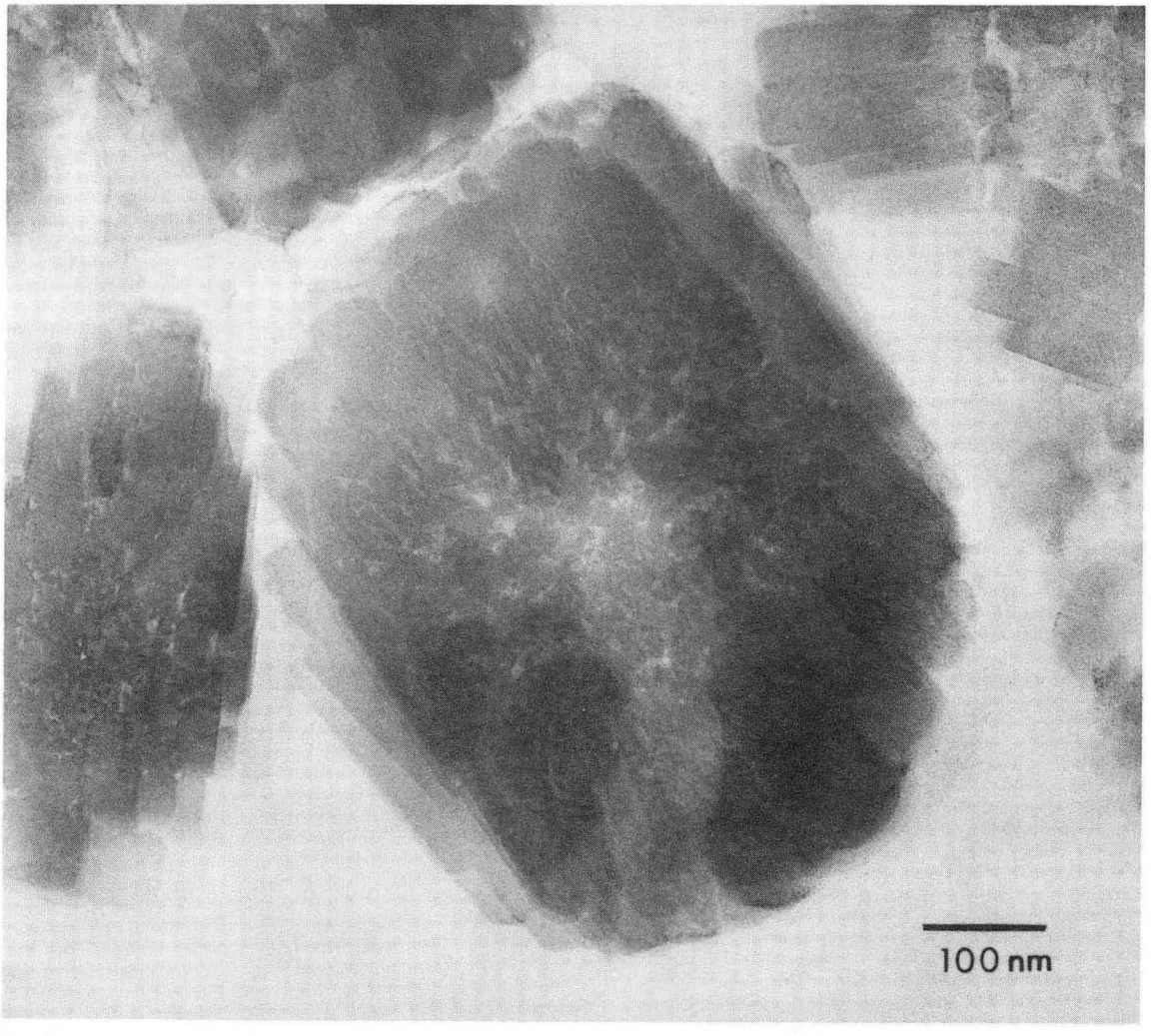

Figure 4.2 - Bright field TEM image of thin section of calcined FeZSM-5 grown from a stirred gel with SiO_2:Fe_2O_3-ratio $\simeq$ 50 showing iron-rich second phase particles on some of the FeZSM-5 particle edges. XBB 870-9599

the FeZSM-5 particle outer edges. Using XES in the VG STEM (described in chapter 3), these second phase particles have been determined to be iron-rich as compared to the FeZSM-5 matrix [29].

Figure 4.3 shows the uniform distribution of second phase particles throughout the FeZSM-5 particles which resulted from steaming at 550 °C for 4 hours the FeZSM-5 particles that had been grown from a stirred gel with SiO_2:Fe_2O_3-ratio $\simeq$ 50. Hydrothermal treatment of all samples grown from stirred gels produced homogeneous distributions of iron-rich second phase particles generally ranging in size from 1.5 to 5 nm for steaming times of 1, 2 or 4 hours at 550 °C. When the stirred FeZSM-5 samples are steamed at 700 °C for 4 hours, the second phase particles range in size from 2.5 to 15 nm (fig. 4.4). Particles 10 nm or larger are often found on the surfaces of the individual FeZSM-5 crystallites within the FeZSM-5 particle; whereas, the smaller second phase particles are homogeneously dispersed throughout the FeZSM-5 particles. The number of second phase particles increases with the iron content of the FeZSM-5 while their size increases with the duration and temperature of the steam treatment. The anomaly to this is the FeZSM-5 sample grown from a gel with SiO_2:Fe_2O_3-ratio $\simeq$ 90 and steamed for 2 hours at 550 °C in which most of the second phase particles are 3 to 6 nm diameter with some 10 nm; this suggests that the temperature of the steam treatment was probably higher than 550 °C since the same sample treated for 4 hours has 2.5 to 4 nm diameter particles.

Prolonged steam treatment, 12 hours at 550 °C, of the FeZSM-5 also results in large second phase particles along grain boundaries and on the surfaces of the FeZSM-5 crystallites (fig. 4.5). Most probably during the long steam treatment, the larger particles on or near the FeZSM-5 internal and external surfaces grow at the expense of the smaller homogeneously distributed second phase particles since few small particles are visible after the

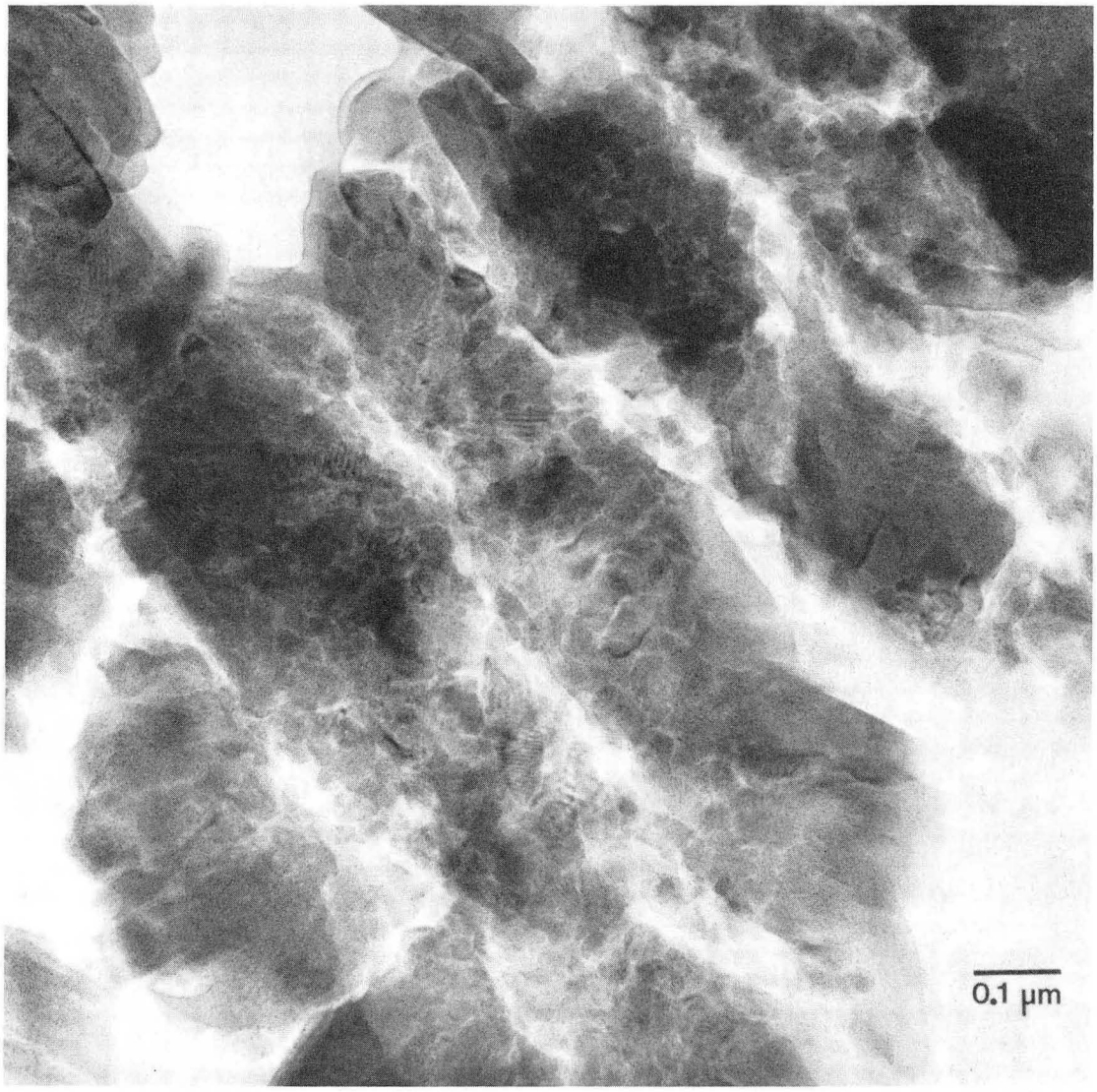

Figure 4.3 - Bright field TEM image of thin section of FeZSM-5 grown from a stirred gel with SiO_2:Fe_2O_3-ratio $\simeq$ 50 after steam treatment at 550 °C for 4 hours showing uniform distribution of iron-rich second phase particles throughout the FeZSM-5 particles. XBB 887-6974

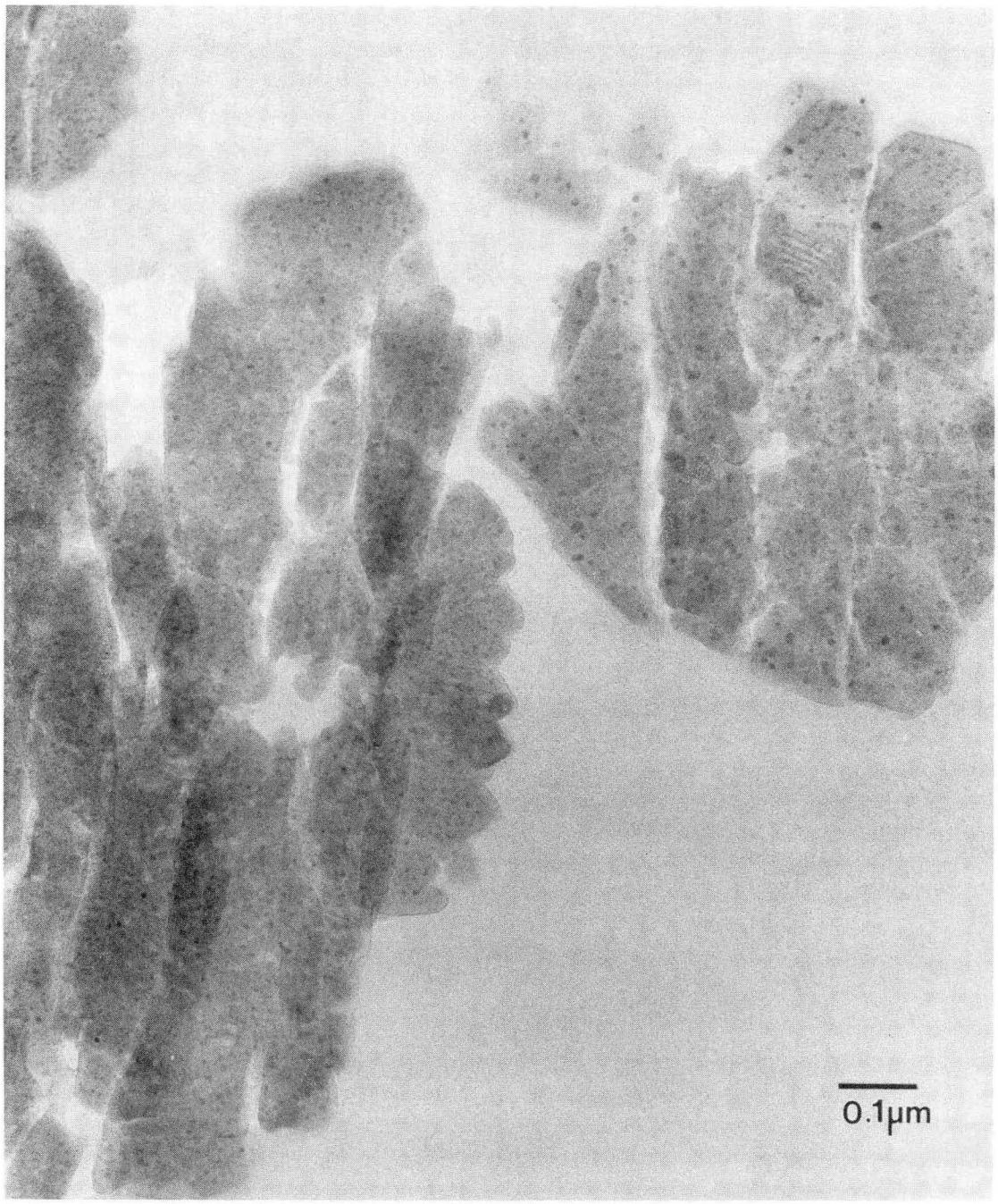

Figure 4.4 - Bright field TEM image of thin section of FeZSM-5 grown from a stirred gel with SiO_2:Fe_2O_3-ratio $\simeq$ 50 after steam treatment at 700 °C for 4 hours showing distribution of second phase particles throughout the FeZSM-5 particles. XBB 887-6973

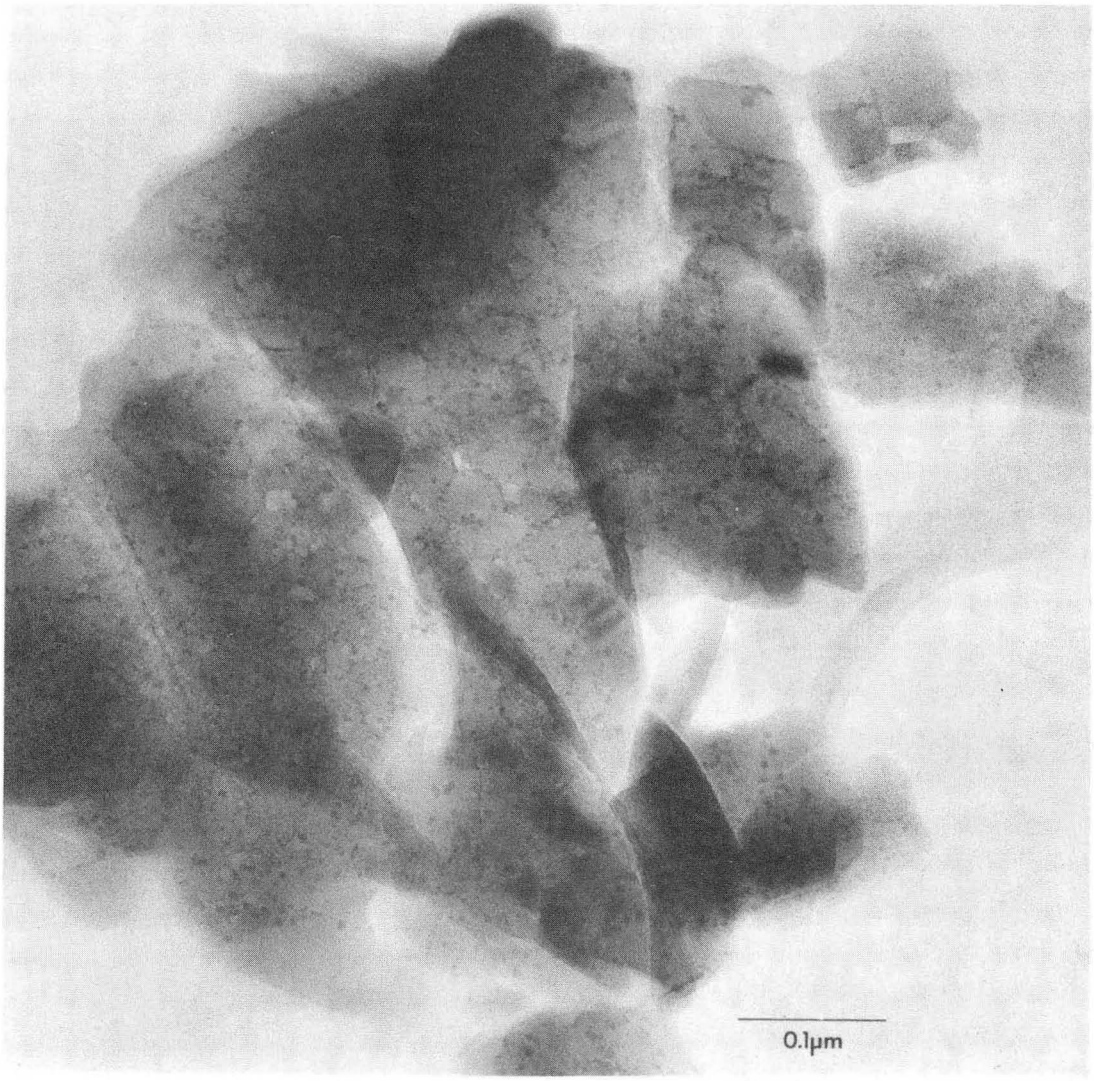

Figure 4.5 - Bright field TEM image of thin section of FeZSM-5 grown from a stirred gel with SiO_2:Fe_2O_3-ratio $\simeq$ 50 after steam treatment at 550 °C for 12 hours showing segregation of second phase particles to grain boundaries and surfaces in and on the FeZSM-5 particles. XBB 886-6201

12 hour treatment.

Molecular sieve particles grown from unstirred gels contain (6-15 nm) voids, some are sharply faceted; typically most of these voids are located in the small, iron-rich crystallites near the center of the FeZSM-5 particle (fig. 4.6). Many of the facets of these voids are rounded during steam treatment, the voids also provide sites for the nucleation and growth of second phase particles (fig. 4.7). Hydrothermal treatments for 1, 2 or 4

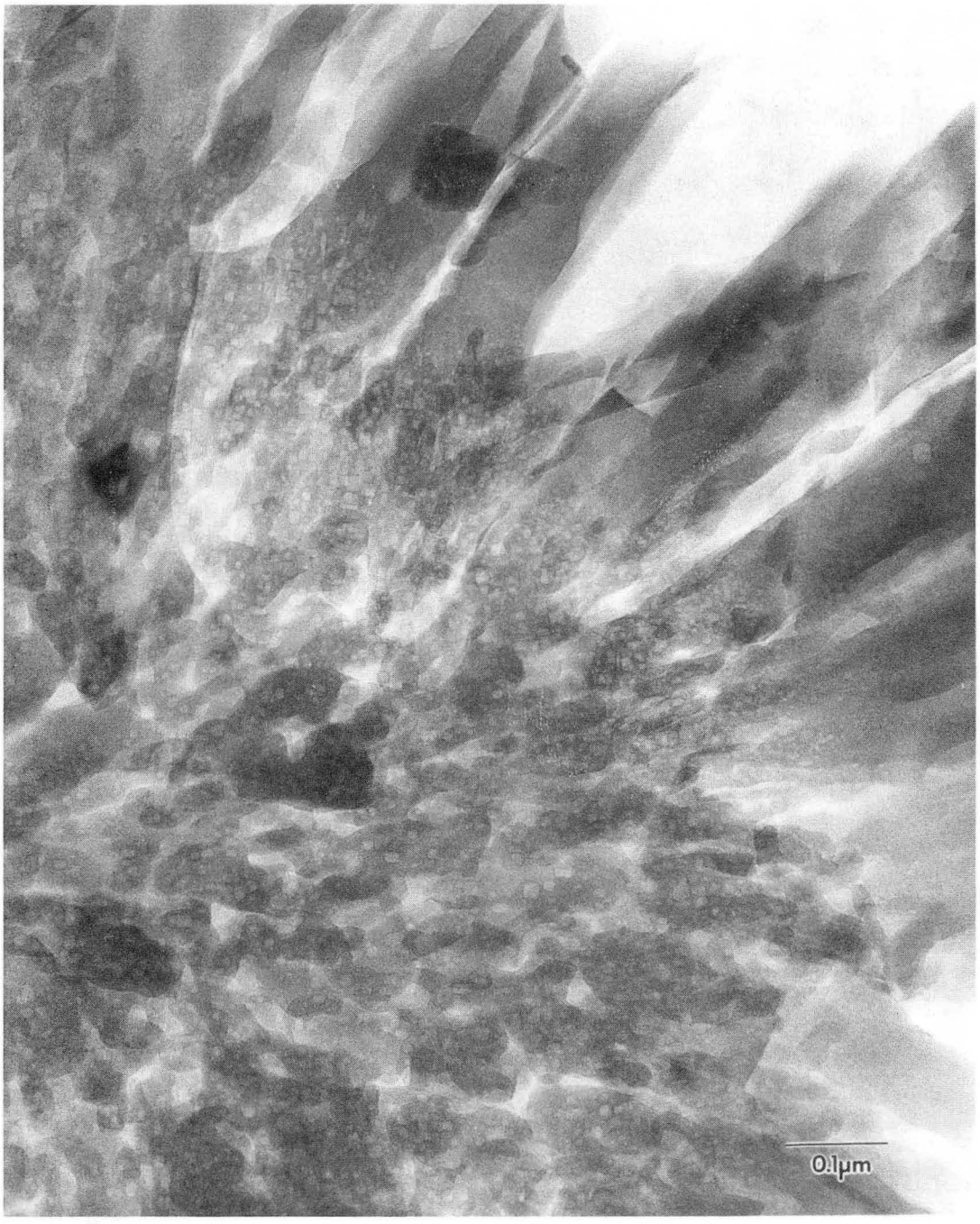

Figure 4.6 - Bright field TEM image of a thin section of a part of an as-synthesized FeZSM-5 particle grown from an unstirred gel with SiO_2:Fe_2O_3-ratio $\simeq$ 50. The center of the FeZSM-5 particle (lower left area of the picture) consists of the small "holey" crystallites of FeZSM-5 and the outer edges are characterized by the larger FeZSM-5 crystals (upper right quadrant of the photograph).

XBB 886-6202

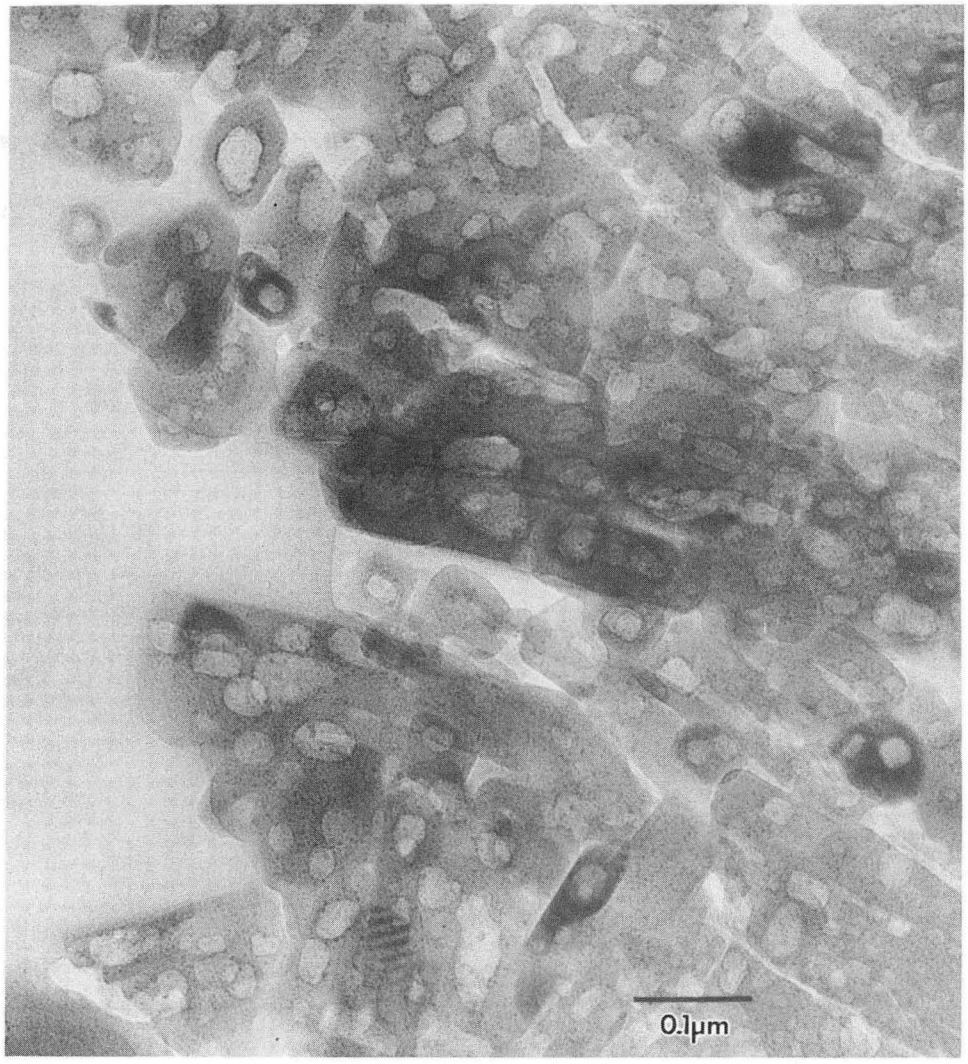

Figure 4.7 - Bright field TEM image of a thin section of the "holey" center portion of a FeZSM-5 particle grown from an unstirred gel with SiO_2:Fe_2O_3-ratio $\simeq$ 50, that has been steam treated at 550 °C for 4 hours. Note that the edges of the voids are rounded and decorated with second phase particles. XBB 882-1491

hours at 550 °C of the unstirred samples produces second phase particles, 2 to 6 nm diameter, whereas steaming at 700 °C for 4 hours results in particles 2.5 to 16 nm in size (Fig. 4.8). The distribution of second phase particles in figure 4.8 illustrates the effects of inhomogeneous iron distribution prior to steaming. The iron-rich center of the FeZSM-5 particle contains a relatively uniform distribution of second phase particles (2.5 - 8 nm) but

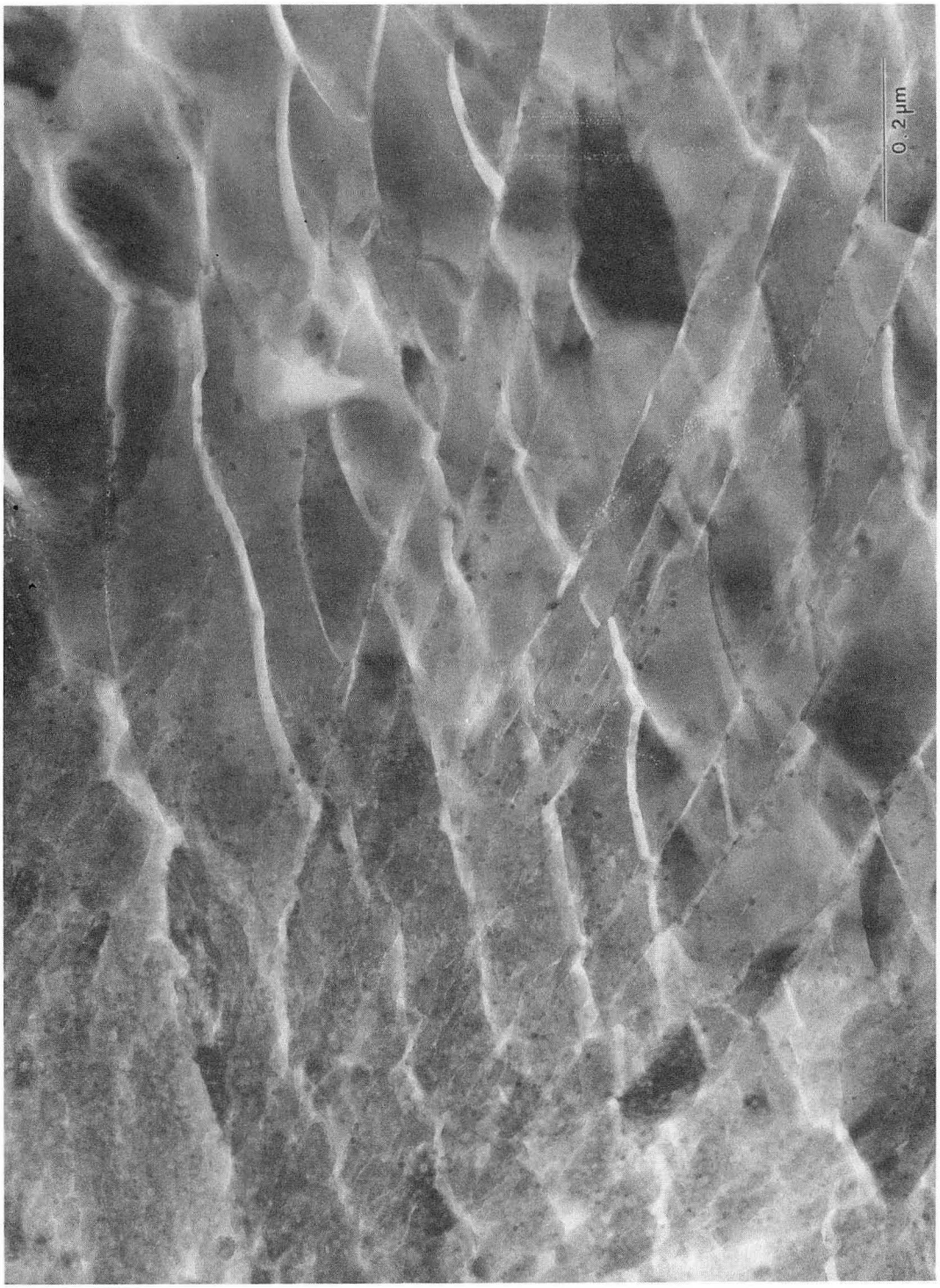

Figure 4.8 - Bright field TEM image of a thin section of a FeZSM-5 particle grown from an unstirred gel with SiO_2:Fe_2O_3-ratio $\simeq$ 200, that has been steam treated at 700 °C for 4 hours. Note the inhomogeneous distribution of second phase particles throughout the FeZSM-5 particle. XBB 886-6204

the second phase is sparsely distributed as larger (7 - 13 nm) particles throughout the larger silicon-rich FeZSM-5 crystallies at the particle edge.

Hydrothermal treatment of unstirred samples consistently resulted in larger second phase particles than did the same treatment of stirred samples. This is probably due to a combination of two contributing factors: a less homogeneous iron distribution in the as-synthesized form of the unstirred samples and enhanced diffusion during steam treatments, perhaps involving the voids.

4.3.2. Microdiffraction and HREM imaging

The iron-rich second phase particles larger than 7.5 nm are crystalline but electron diffraction is very weak and diffuse due to their small size. Conventional selected area diffraction yields only the ZSM-5 framework structure spots. Microdiffraction, obtained by focusing a 20 nm electron probe onto the area from which diffraction is desired, applied to the second phase particles yields identifiable electron diffraction patterns (Fig. 4.9 and 4.10). The patterns in figure 4.9 are from well separated, larger particles in the FeZSM-5 sample, steamed for 4 hours at 700 °C, grown from a stirred gel with SiO_2:Fe_2O_3-ratio $\simeq$ 200. In addition to these diffraction patterns, the sample grown from a stirred gel with SiO_2:Fe_2O_3-ratio $\simeq$ 50 after the same steam treatment also contains particles which produce the diffraction patterns in figure 4.10. Microdiffraction on the small ($\leq$ 5 nm) second phase particles shown in figure 4.3 shows only diffuse scattering, no Bragg spots, indicating that the small particles are amorphous. After prolonged hydrothermal treatment, however, the second phase particles (shown in figure 4.5) show some weak diffraction spots but not any strong two dimensional patterns.

Since the steam treatments are performed on the ammonium form of the iron silicate, only iron oxides, hydroxides and iron silicate structures are considered as possible

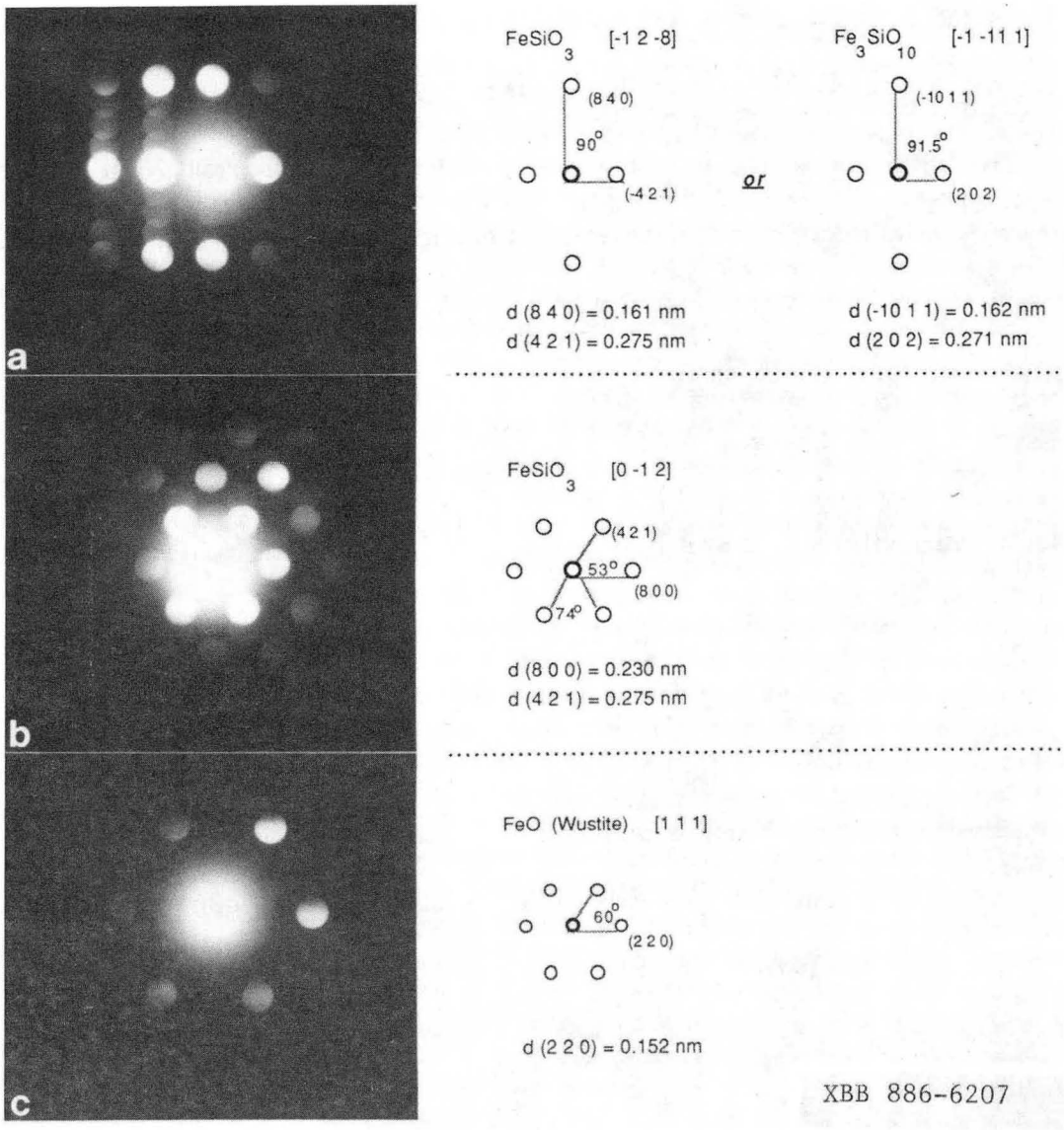

Figure 4.9 - Electron diffraction patterns and most probable indexing schemes from some second phase particles in the steam treated (700 °C for 4 hours) FeZSM-5 particles grown from a stirred gel with SiO_2:Fe_2O_3-ratio $\simeq$ 200.

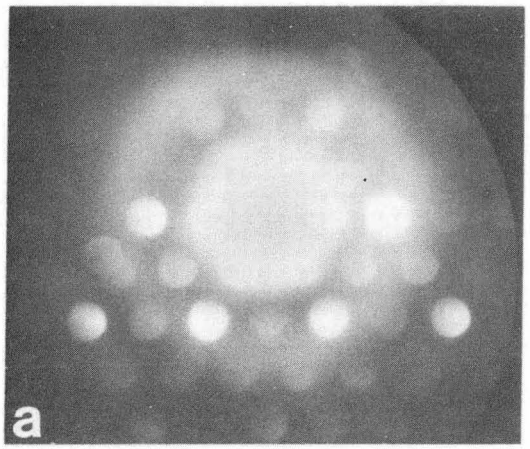

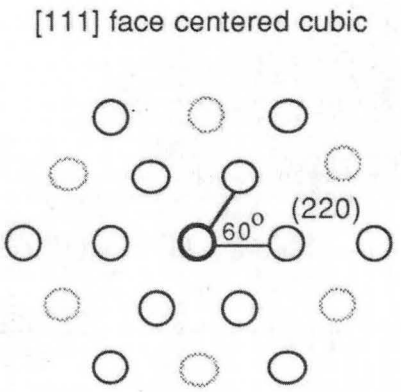

measured

d (220) = 0.285 ± 0.01

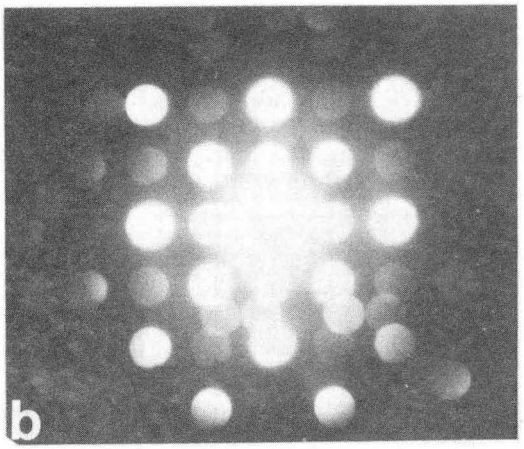

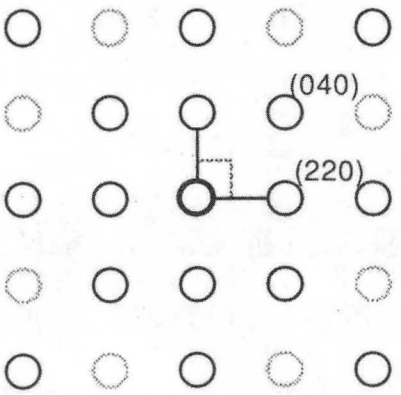

measured

d (220) = 0.285 ± 0.01

d (400) = 0.205 ± 0.01

XBB 889-8741

Figure 4.10 - Indexed electron diffraction patterns from some of the second phase particles in steam treated (700 °C for 4 hours) FeZSM-5 particles originally grown from a stirred gel with SiO_2:Fe_2O_3-ratio $\simeq$ 50.

identities for the second phase particles. The pattern shown in figure 4.9a may be indexed as the [$\bar{1}$ $\bar{1}\bar{1}$ 1] zone of Fe_3SiO_{10} if the weak spots between the transmitted beam and the $\bar{1}0$ 1 1 spot are ignored. A more consistent indexing of this pattern is achieved using $FeSiO_3$ in the [$\bar{1}$ 2 $\bar{8}$] zone; in this choice the weak spots consistently index as 2 1 0 reflections. Figure 4.9b can be indexed only as $FeSiO_3$ in the [0 $\bar{1}$ 2] direction which increases the confidence that the diffraction pattern in figure 4.9a is correctly identified as [$\bar{1}$ 2 $\bar{8}$] $FeSiO_3$. For the pattern in figure 4.9c only one solution seems possible, the [1 1 1] zone of wustite (FeO).

After prolonged electron beam exposure, the molecular sieve structure is damaged and becomes amorphous, facilitating high resolution electron microscopy (HREM) images of the second phase particles. In figure 4.11 two sets of lattice planes of the second phase particle with spacing 0.27 nm intersect with a 74 ° angle between them. This is the HREM image that would be expected for the [0 $\bar{1}$ 2] zone of $FeSiO_3$, adding confidence to the assignment of the $FeSiO_3$ indexing to the diffraction pattern in figure 4.9a.

The electron diffraction pattern in figure 4.10a may be indexed as the [1 1 1] zone of face centered cubic Fe_2SiO_4, Fe_3O_4 (magnetite), γ-Fe_2O_3 (maghemite) or as $Fe(OH)_3$. These four structures can not be differentiated solely by electron diffraction since all four have very similar lattice parameters; a_0 = .8235 nm (Fe_2SiO_4), a_0 = .8396 nm (Fe_3O_4), a_0 = .8350 (γ-Fe_2O_3) and a_0 = .837 nm ($Fe(OH)_3$). Figure 4.10b shows a [0 0 1] zone diffraction pattern that also can be identified as resulting from a face centered cubic material, either the iron silicate, the iron oxides or the iron hydroxide.

Although electron diffraction cannot distinguish between the oxide, hydroxide or silicate structures, other information can be used to eliminate some of the choices. It is well documented that hydroxide compounds and hydrated compounds change structure under

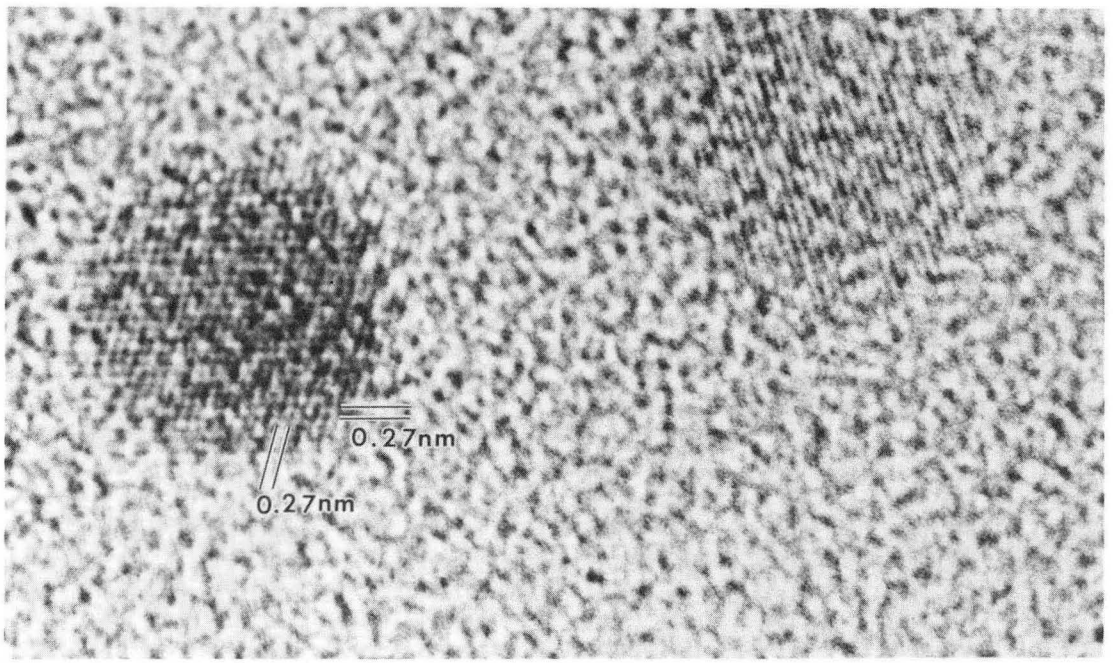

Figure 4.11 - High resolution phase contrast TEM image of second phase particles in a steam treated (550 °C for 2 hours) FeZSM-5 particle grown from a stirred gel with SiO_2:Fe_2O_3-ratio $\simeq$ 90. Note the molecular sieve structure is amorphous due to electron beam damage facilitating the imaging of the lattice structure of the second phase particles. XBB 886-6200

the electron beam [40 - 43]; typically they dehydrate to the oxide. On this basis, the $Fe(OH)_3$ can not be responsible for the diffraction patterns in figure 4.10; microdiffraction requires a large electron flux to the specimen which would result in change of the iron hydroxide structure probably to an iron oxide (or amorphous) phase. By the same rational if maghemite is responsible for the diffraction patterns, then lepidocrocite, FeO(OH), may have been formed during the hydrothermal treatment and probably transformed to Fe_2O_3 by dehydration under the intense electron beam.

Thermodynamic phase equilibria considerations allow for the formation of either of the iron oxides or the iron silicate [44, 45]; however, γ-Fe_2O_3 is metastable with respect to α-Fe_2O_3 and will rapidly transform at 400 °C from light brown maghemite to dark red

α-Fe_2O_3, hematite [46]. Therefore γ-Fe_2O_3 would not be expected in the FeZSM-5 sample producing the diffraction patterns in figure 4.10 since this sample had been steamed at 700 °C. Subsequent heat treatment in air at 450 °C confirms that maghemite is not present in this sample in sufficient quantity to cause a color change of the sample with its transformation to hematite. This argument alone is not sufficient to eliminate maghemite as the phase giving the diffraction patterns since the color of a phase containing iron depends on its particle size and its dispersion in addition to its concentration [47].

Since microdiffraction is specific and representative only of the individual particles probed, the statistics of the analysis are important. The microdiffraction patterns shown are representative only of the larger second phase particles, since the smaller ones produced diffraction patterns characteristic of amorphous material. In the 4 hour 700 °C steamed FeZSM-5 sample grown from a stirred gel with SiO_2:Fe_2O_3-ratio $\simeq$ 200, 41% of the large second phase particles probed by microdiffraction gave the pattern in figure 4.9a, 32% gave that in figure 4.9b and 5% gave the wustite pattern in figure 4.9c. In the similarly steamed sample grown from a stirred gel with four times as much iron, 21% of the second phase particles gave the diffraction pattern in figure 4.9a, 14% yielded that in figure 4.9b, 7% gave figure 4.9c, 14% gave figure 4.10a and 21% gave figure 4.10b. Other particles in both samples produced incomplete or overlapping diffraction patterns that could not be identified. In all, 78% of the patterns recorded by microdiffraction were identified, in reality these particles probably are characteristic of about 30% of the second phase particles, since most of the particles are smaller and amorphous; hence the identity of these smaller particles is unclear.

Both high resolution imaging and microdiffraction indicate that some of the second phase particles contain iron is in the 2+ oxidation state, e.g., $FeSiO_3$ and FeO (and possi-

bly Fe_2SiO_4 and Fe_3O_4). This contradicts the Mössbauer data on these materials [17], which indicates the presence of iron in the 3+ oxidation state mostly (~85%) in octahedral coordination and a small amount (~15%) in tetrahedral environment. Since the smaller particles are a different structure and are generally more numerous, it is probable that the Mössbauer data is only sensitive to the larger volume fraction of the material in the smaller particles, as Mössbauer is a bulk technique. Thus the identification of some of the large second phase particles as structures containing iron in its 2+ oxidation state is valid although it is not corroborated by the Mössbauer results.

Although it would be valuable to positively identify the second phase particles formed by hydrothermal treatment so that a mechanism for their formation and growth could be understood, it is not essential to its use as a catalyst. Fischer-Tropsch reactions occur in a reducing atmosphere and the actual iron catalyst is probably a reduced iron compound that could only exist under the reaction conditions.

4.4. Summary

Transmission electron microscopy imaging of a thin section of FeZSM-5 particles reveals that they are aggregates of smaller FeZSM-5 crystallites. Unstirred gels produce aggregates with small crystals in the center surrounded by larger crystals, while the agglomerates from stirred gels are formed without size or shape discrimination.

Thermal and hydrothermal treatments lead to the formation and growth of iron-rich second phase particles in the FeZSM-5 particles. Second phase particles range in size from 1.5 nm to 6 nm for 1, 2 or 4 hour 550 °C steam treatments and 5 nm to 16 nm for 4 hour 700 °C treatments. These particles are homogeneously dispersed throughout the FeZSM-5 particles grown form stirred gels. Overall in the FeZSM-5 particle agglomerates grown from unstirred gels, the second phase particles are larger than in the stirred

samples with the smaller second phase particles relatively uniformly distributed at the agglomerate center and the larger ones are predominately located between FeZSM-5 crystallites nearer to the aggregate edges.

Microdiffraction shows that the second phase particles larger then 7.5 nm are crystalline while smaller particles are amorphous. The identity of the particles differs with the temperature and duration of the steam treatments and probably on the amount of iron in the FeZSM-5 before steaming. Samples of FeZSM-5 steamed at 550 °C for 1, 2 or 4 hours generally contain only amorphous second phase particles; after 12 hours at 550 °C some crystallinity is observed in the iron-rich second phase. Hydrothermal treatment at 700 °C leads to many crystalline second phase particles. Some of them are $FeSiO_3$ and FeO; and some Fe_2SiO_4, Fe_3O_4, γ-Fe_2O_3 and γ-FeO(OH) are probably also present.

CHAPTER 5

CATALYTIC PERFORMANCE OF FeZSM-5

These iron silicate molecular sieves are intended for use as Fischer-Tropsch catalysts for the conversion of carbon monoxide and hydrogen to gasoline range hydrocarbons. Since Fischer-Tropsch reactions typically produce complex mixtures of hydrocarbons the activity and selectivity of the catalyst is difficult to assess directly. For initial characterization purposes, the catalytic probe reaction, dehydrogenation of ethyltoluene to methylstyrene, is used to test the catalytic activity and selectivity of the calcined and hydrothermally treated FeZSM-5 samples grown from stirred gels [16], (fig. 5.1).

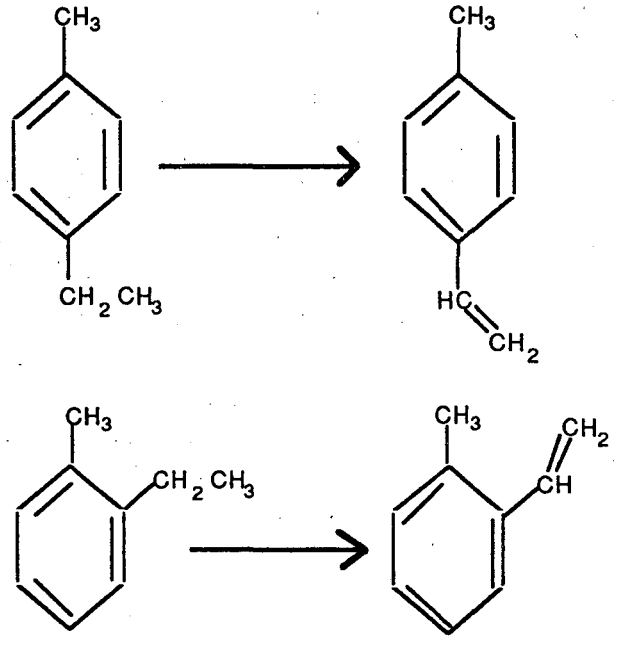

Figure 5.1 - Dehydrogenation reactions of para-ethyltoluene to para-methylstyrene and ortho-ethyltoluene to ortho-methylstyrene.

5.1. Background: the probe reaction

A probe reaction must be simple, occur over an iron oxide phase and be shape selective, i.e., it must be able to distinguish between the catalytic iron phase within the pore system and the catalytic iron phase outside the ZSM-5 structure. As shown in table 5.1, the conversion of ethyltoluene to methylstyrene is catalyzed by iron oxide but not by the silica form of the ZSM-5, silicalite, therefore this reaction readily meets the first two criteria for a good probe reaction. The para forms of ethyltoluene and methylstyrene readily diffuse through the pores of the ZSM-5 structure, but the ortho isomers are physically impeded. Therefore conversion of the para-ethyltoluene can occur both inside and outside the ZSM-5 pore structure while the conversion of the ortho-ethyltoluene can occur only on the outside of the ZSM-5 particles, thus the reaction is shape selective. Catalytic activity is simply measured by the amount of conversion to products, whereas the shape selectivity of the FeZSM-5 catalyst is reflected by the ratio of the rate of conversion of the para compared to the rate of conversion of the ortho form.

Table 5.1 - Conversion rates for ethyltoluene to methylstyrene

Sample	Production rate in $\frac{\text{ng moles}}{\text{g catalyst sec}}$		$\frac{\text{para}}{\text{ortho}}$ conversion ratio
	Para-isomer	Ortho-isomer	
Unsupported iron oxide	11.3	7.4	1.5
Silicalite	0.6	0.6	

5.2. Results and discussion

The rates of methylstyrene produced from the dehydrogenation of ethyltoluene (in nanogram moles per gram catalyst second) are shown in tables 5.1 and 5.2 for the FeZSM-5 catalysts grown from stirred gels [16]. All calcined forms show activity for the

reactions indicating that thermal treatment, intended only to remove the crystal directing agent, results in catalytic activation probably by removal of some of the iron from the FeZSM-5 framework. The FeZSM-5 grown in the gel with the SiO_2:Fe_2O_3-ratio $\simeq$ 50 shows the highest activity for conversion by the calcined forms. Its conversion rate for the para-ethyltoluene is actually peaked and remains constant after subsequent steam treatment, however the rate of conversion of the ortho isomer increases with steaming at 550 °C. This indicates that hydrothermal treatment at 550 °C causes the migration of catalytically active iron from inside the ZSM-5 pore system to the outside of the FeZSM-5 particles where it is able to react with the ortho-ethyltoluene. The process of migration of catalytic iron to the outside of the pore system is more pronounced at elevated temperatures, indicated by the drop in conversion rate of the para isomer for the 4 hour steaming at 700 °C; agglomeration of the external iron is reflected in the sharply lower conversion rate for the ortho-ethyltoluene for the same hydrothermal treatment.

These catalytic measurements are in good agreement with the data provided by the transmission electron microscope images shown in the previous chapter. Only this high iron content sample showed some small iron-rich second phase particles following thermal treatment. When steam treated at 550 °C, the TEM images showed 3 to 5 nm second phase particles for 1, 2 or 4 hour steamings with the longer times favoring the slightly larger particles, generally occurring on the molecular sieve particle boundaries. Images after hydrothermal treatment at 700 °C showed larger second phase particles outside the ZSM-5 crystallites, in addition to the 3 to 6 nm particles throughout the ZSM-5 particles, indicating the migration of iron and its agglomeration on the surface of the molecular sieve particles.

Table 5.2 - Conversion rates using para-ethyltoluene as feed

Stirred gel with SiO_2:Fe_2O_3	Rate of methylstyrene produced in $\frac{\text{ng moles}}{\text{g catalyst sec}}$				
	Calcined	550 °C steam			700 °C steam
		1 hour	2 hours	4 hours	4 hours
200	2.2	10.4	15.8	16.2	14.9
90	19.2	25.3	29.4	29.5	18.4
50	40.9	40.6	39.9	39.8	22.9

Table 5.3 - Conversion rates using ortho-ethyltoluene as feed

Stirred gel with SiO_2:Fe_2O_3	Rate of methylstyrene produced in $\frac{\text{ng moles}}{\text{g catalyst sec}}$				
	Calcined	550 °C steam			700 °C steam
		1 hour	2 hours	4 hours	4 hours
200	1.3	5.0	9.0	9.8	7.2
90	7.9	10.8	13.3	13.6	8.7
50	12.1	16.0	16.7	16.7	6.6

The catalytic activity for the FeZSM-5 grown with SiO_2:Fe_2O_3-ratio $\simeq$ 200 increases significantly with steaming at 550 °C for 1 and 2 hours but remains relatively constant with longer treatments. These data are in accord with the TEM images that detect second phase particles only after 2 hours of 550 °C steaming indicating that more iron has left the ZSM-5 framework and aggregated to form catalytically active second phase particles. This migration and agglomeration of the catalytically active iron is indicated by the drop in the conversion rates for both the para and ortho isomers and by the larger second phase particles seen in the TEM images. As expected the reaction data for the sample with SiO_2:Fe_2O_3-ratio $\simeq$ 90 falls between the high and low iron containing samples.

The shape selectivity of the FeZSM-5 catalysts is assessed by comparing the rate of conversion occurring inside the pore system to that occurring outside the ZSM-5 pores; in this case, it is the ratio of the conversion rate for the para isomer compared to that of the ortho isomer and is summarized in table 5.4.

Table 5.4 - Selectivity of FeZSM-5 catalysts

Stirred gel with SiO_2:Fe_2O_3	Ratios of $\frac{\text{para}}{\text{ortho}}$ conversion rates				
	Calcined	550 °C steam			700 °C steam
		1 hour	2 hours	4 hours	4 hours
200	1.7	2.1	1.8	1.8	2.1
90	2.4	2.3	2.2	2.2	2.1
50	3.4	2.5	2.4	2.4	3.5

Overall the rate of conversion for the para-ethyltoluene is slightly more than twice that for the ortho isomer. The lowest iron content sample shows the least shape selectvity with the para to ortho ratio between 1.7 and 2.1, only slightly larger than the para to ortho ratio of unsupported iron oxide. This is not entirely unexpected and can be understood by considering what happens to the iron after it leaves the molecular sieve framework. The iron leaves the framework and diffuses through the pores until it reaches the particle surface or it encounters another diffusing iron species and forms a larger iron species, whichever occurs first. In the case of the silica-rich FeZSM-5 materials, the iron is more likely to reach the surface before colliding with another iron and forming a nondiffusable entity.

The high iron content sample, grown with SiO_2:$Fe_2O_3 \simeq 50$, shows not only the highest catalytic activity but also the largest degree of shape selectivity with para to

ortho conversion rate ratios between 2.4 to 3.5. Selectivity is high for both the calcined form and for the 700 °C steamed samples, but it is significantly lower for the samples steamed at 550 °C for 1 to 4 hours. Although thermal treatment is used to remove the crystal directing agent, it is clear from the TEM images that in the case of this high iron content sample a sizeable portion of the iron leaves the framework and forms second phase particles; the larger ones are visible in TEM images. Most of the smaller, invisible particles are located inside the FeZSM-5 particles and catalyze the conversion of the para-ethyltoluene. During subsequent steam treatment the iron species migrate to the surface and agglomerate into large particles and the iron-rich particles inside the ZSM-5 crystals also continue to grow. Those iron-rich particles on the surface account for the increased conversion of the ortho-ethyltoluene and the decreased selectivity of the samples steamed at 550 °C. Hydrothermal treatment at 700 °C results in high shape selectivity although some of the iron-rich second phase particles are quite large, over 10 nm diameter; this is due to the location of the larger particles on the outside the ZSM-5 particles. Much of the iron moves out of the pore system during steaming at 700 °C, thus the activity for conversion of the para isomer inside the ZSM-5 pore structure is reduced. One might expect this enrichment of the surface with catalytic iron to increase the conversion of the ortho isomer, however this iron agglomerates on the surface and forms large second phase particles thus lowering the surface to volume ratio of the active iron catalyst resulting in reduced conversion of the ortho-ethyltoluene and hence the catalyst exhibits high shape selectivity.

5.3. Summary

Good agreement has been found between the microstructural details of the FeZSM-5 catalysts and their catalytic performance. Catalytic activity increases with an increase in the iron content due to a larger amount of the catalytically active phases. Catalytic activity and shape selectivity remain relatively constant during 1 to 4 hours of hydrothermal treatment at 550 °C. Shape selectivity is greatest for the high iron content sample following high temperature steam treatment where the iron that is outside the ZSM-5 particles agglomerates into 10 nm and larger sized particles. This lowers the surface to volume ratio, minimizing the conversion of the ortho isomer and results in a good shape selective catalyst.

CHAPTER 6

CONCLUSIONS

SEM has shown that stirring the gel during crystal growth results in small (0.5 μm - 1 μm) molecular sieve particle aggregates. The particle morphology changes from regular spheres to irregular spheres and cubes as the iron content increases; this is analogous to the effect of increasing the aluminum content in ZSM-5 zeolites. Crystal growth without agitation produces some single crystals in addition to the micron or larger sized particle aggregates. The addition of alkali cations during unstirred crystal growth leads to larger particle agglomerates and generally more single crystals of FeZSM-5.

In the iron silicate FeZSM-5, stirring the gels during crystal growth promotes a homogeneous iron distribution throughout the particles, both on the intra- and inter-particle scales. Particles grown from unstirred gels have consistently higher concentrations of iron in the center of the particles and are silica-rich near the particle edges. This is consistent with the aluminosilicate ZSM-5 system, where the distribution of aluminum in the ZSM-5 crystals varies from particles with aluminum-rich centers to homogeneous particles to particles with silicon-rich centers, depending on growth conditions [48, 49, 50, 24, 51]. When the zeolite ZSM-5 is a minor product phase, the major phase is aluminum-rich and the center of the ZSM-5 crystals are silica-rich and the surface of the crystals is aluminum-rich [48, 49, 51]. If the ZSM-5 is the major or only product phase, the aluminum is uniformly distributed or shows some enrichment at the interior of the crystal [51].

Iron-rich second phase particles form and grow throughout the molecular sieve crystals during thermal and hydrothermal treatments of the iron silicate, FeZSM-5. The size

of the second phase particles is strongly dependent on the temperature of the steam treatment and to a lesser extent the duration of the treatment. The spatial distribution of the second phase particles depends strongly on whether the molecular sieve crystals were grown from stirred or unstirred gels. Those grown from stirred gels have a uniform distribution of second phase particles throughout the ZSM-5 particles with steam times up to 4 hours; only after treatment for 12 hours do they begin to show segregation to ZSM-5 particle interfaces. The steamed FeZSM-5 particles grown from unstirred gels show a heterogeneous second phase particle distribution indicative of their iron concentration profile prior to hydrothermal treatment; many 4 to 6 nm particles are uniformly dispersed throughout the center of the FeZSM-5 particles, whereas 10 nm and larger particles are found between the FeZSM-5 crystallites nearer the FeZSM-5 particle edges.

Microdiffraction shows that the second phase particles larger then 7.5 nm are crystalline while smaller particles are amorphous. Hydrothermal treatment at 700 °C leads to many crystalline second phase particles; $FeSiO_3$ and FeO have been positively identified and at least one other phase, probably γ-Fe_2O_3 or γ-FeO(OH), is also present.

Second phase particle size and spatial distributions affect the catalytic activity and selectivity of the FeZSM-5 catalysts. Increases in the iron concentration result in increases in the amount of active second phase and hence the catalytic activity increases. High activity with the best shape selectivity is achieved with the high iron concentration sample steamed for 4 hours at 700 °C. This is readily explained by the size and spatial distributions of the second phase particles; small second phase particles are evenly distributed throughout the FeZSM-5 particles and the larger particles are found outside the FeZSM-5 crystallites, thus the activity inside the crystallites remain high while the activity outside the ZSM-5 structure is minimized.

Although the Fischer-Tropsch synthesis using these catalysts is the subject of future work, this research has taken the first steps in the promising future of shape selective active iron silicate catalysts. Crystal growth from stirred gels with moderate to high concentrations of iron results in uniform size and shape iron silicate FeZSM-5 particles with a homogeneous distribution of iron throughout. Hydrothermal treatment of this iron silicate results in an active shape selective bifunctional catalyst, with an active iron phase in a shape selective molecular sieve matrix.

REFERENCES

[1] Kokotailo, G.T., Lawton, S.L., Olson, D.H., and Meier, W.M., Nature, **272**, 437 (1978).

[2] Anderson, J.R., Foger, K., Mole, T., Rajadhyaksha, R.A., and Sanders, J.V., J. Catal., **58**, 114 (1979).

[3] Dejaifve, P., Vedrine, J.C., Bolis, V., and Derouane, E.G., J. Catal., **63**, 331 (1980).

[4] Olson, D.H., Kokotailo, G.T., Lawton, S.L., and Meier, W.M., J. Phys. Chem., **85**, 2238 (1981).

[5] Ione, K.G., Echevskii, G.V., and Nosyreva, G.N., J. Catal., **85**, 287 (1984).

[6] Chen, N.Y., and Garwood, W.E., Catal. Rev. -Sci. Eng., **28**, 185 (1986).

[7] Chang, C.D., Lang, W.H., and Silvestri, A.J., J. Catal. **56**, 268 (1979).

[8] Chang, C.D., and Silvestri, A.J., J. Catal. **47**, 249 (1977).

[9] Caesar, P.D., Brennan, J.A., Garwood, W.E., and Ciric, J., J. Catal. **56**, 274 (1979).

[10] Iton, L.E., Beal, R.B., and Hodul, D.T., J. Molec. Catal. **21**, 151 (1983).

[11] Kotasthane, A.N., Shiralkar, V.P., Hegde, S.G. and Kulkarni, S.B., Zeolites **6**, 396 (1986).

[12] Shamsi, A., Rao, V.U.S., Gormley, R.J., Obermyer, R.T., Schehl, R.R., and Stencel, J.M., Appl. Catal. **27**, 55 (1986).

[13] Szostak, R., and Thomas, T.L., J. Catal. **100**, 555 (1986).

[14] Sheldon, R.A., "Chemicals from Synthesis Gas" D. Reidel Publishing Company, Holland, pp. 64-73 (1983).

[15] Szostak, R., Nair, V., and Thomas, T.L., J. Chem. Soc. Faraday, **83**, 487 (1987).

[16] Nair, V., PhD Thesis, Georgia Institute of Technology, Atlanta, GA, 1987.

[17] Meagher, A., Nair, V., and Szostak, R., Zeolites, **8**, 3 (1988).

[18] Hayat, M.A., "Introduction to Biological Scanning Electron Microscopy" University Park Press, Baltimore, MD, pp 1-78 (1978).

[19] Ruedl, E., and Valdre, U., eds., "Electron Microscopy in Materials Science" Commission of the European Communities, Luxemburg, pp 1187-1198 (1975).

[20] Goldstein, J.I., and Yakowitz, H., eds., "Practical Scanning Electron Microscopy" Plenum, New York (1975).

[21] Nastro, A. and Sand, L.B., Zeolites **3**, 57 (1983).

[22] Williams, D.B., *Practical Analytical Electron Microscopy in Materials Science,* Philips Electronic Instruments, Inc., New Jersey, (1984).

[23] *Introduction to Analytical Electron Microscopy,* eds. Hren, J.J., Goldstein, J.I., and Joy, D.C., Plenum Press, New York, (1979).

[24] Lyman, C.E., Betteridge, P.W., and Moran, E.F., in *Intrazeolite Chemistry,* (American Chemical Society, Washington, D.C., 1983), pp.199-215.

[25] Ried, N., in *Practical Methods in Electron Microscopy, V3, Ultramicrotomy,* ed. Glauert, A.M., (Elsevier Science, New York, 1975).

[26] Csencsits, R., Schooley C., and Gronsky, R., J. Electr. Microsc. Tech. **2**, 643 (1985).

[27] Csencsits, R. and Gronsky, R., in *Specimen Preparation for Transmission Electron Microscopy of Materials,* eds. Bravman, J.C., Anderson, R.M., and McDonald, M.L., (Mater. Res. Soc. Proc. **115**, Pittsburgh, PA, 1988) p. 103.

[28] Csencsits, R., Gronsky, R., Nair, V., and Szostak, R., in *Microstructure and Properties of Catalysts,* eds. Treacy, M.M.J., Thomas, J.M., and White, J.M., (Mater. Res. Soc. Proc. **111**, Pittsburgh, PA, 1988) p. 155.

[29] Csencsits, R., Lyman, C.E., and Gronsky, R., *Proc. of the 46th Annual Electr. Microsc. Soc. of Amer. Meeting,* ed. Bailey, G.W., (San Francisco Press, San Francisco, CA, 1988) p. 712.

[30] Kundmann, M.K., PhD thesis, University of California, Berkeley, CA (1988).

[31] Thomas, G., and Goringe, M.J., *Transmission Electron Microscopy of Materials,* John Wiley and Sons, New York (1979).

[32] Edington, J.W., *Monographs in Practical Electron Microscopy in Materials Science,* Philips Electronic Instruments, Mahwah, New Jersey (1974).

[33] Spence, J.C.H., *Experimental High Resolution Electron Microscopy,* Oxford University Press, Oxford (1981).

[34] Scherzer, O., J. Appl. Phys., **20**, 20 (1949).

[35] Bursill, L.A., Lodge, E.A., and Thomas, J.M., Nature, **286**, 111 (1980).

[36] Bursill, L.A., Thomas, J.M., and Rao, K.J., Nature, **289**, 157 (1981).

[37] Treacy, M.M.J., and Newsam, J.M., Ultramicroscopy, **23**, 411 (1987).

[38] Csencsits, R., and Gronsky, R., Ultramicroscopy, **23**, 421 (1987).

[39] Csencsits, R., and Gronsky, R., Zeolites, **8**, 122 (1988).

[40] Hobbs, L.W., Electr. Microsc. Soc. of Amer. Bulletin **15**, 51 (1985).

[41] Hobbs, L.W., Ultramicroscopy **23**, 339 (1987).

[42] Dahmen, U., Kim, M.G., and Searcy, A.W., Ultramicroscopy **23**, 365 (1987).

[43] Van Landuyt, J., Van Tendeloo, G., and Amelinckx, S., Ultramicroscopy **23**, 371 (1987).

[44] Kingery, W.D., Bowen, H.K., and Uhlmann, D.R., *Introduction to Ceramics,* John Wiley and Sons, New York, 283-300 (1976).

[45] Garrels, R.M., and Christ, C.L., *Solutions, Minerals and Equilibria*, Freeman, Cooper and Company, San Francisco, 146-151, 182-197 (1965).

[46] Brindley, G.W., *X-ray Identification and Crystal Structures of Clay Minerals*, The Mineralogical Society, London, 244-265, (1951).

[47] Rossmann, G.R., American Mineralogist **60** 698 (1975).

[48] von Ballmoos, R., and Meier, W.M., Nature, **289**, 782 (1981).

[49] Chao, K., and Chern, J., Zeolites, **8**, 82 (1988).

[50] Derouane, E.G., Gilson, J.P., Gabelica, Z., Mousty-Desbuquoit, C., and Verbist, J., J. Catal., **71**, 449 (1981).

[51] Debras, G., Gourgue, A., Nagy, J.B., and DeClippeleir, G., Zeolites, **5**, 369 (1985).

APPENDIX A

Appendix A - Zeolites

This is a synopsis of some of the information contained in the books and papers listed in the bibliography at the end of this section, to which the reader is referred for in-depth study.

Zeolites are crystalline, hydrated aluminosilicates with alkali and alkaline earth cations. They lose and gain water reversibly and exchange cations without major change of structure. Zeolites were discovered in 1756 by the Swedish mineralogist, Freiherr Axel Fredrick Cronstedt, who named them from the Greek words $\zeta\epsilon\iota\upsilon$ and $\lambda\iota\theta\sigma\sigma$, "boiling stones," in allusion to their peculiar frothing character when heated. This distinguished them as a separate type of silicate mineral, and to date, more than 40 distinct naturally occurring and 100 synthetic zeolites have been identified.

Chemical composition

Zeolites are tektosilicates forming three dimensional frameworks of SiO_4^{-4}, where all the oxygen are shared by adjacent tetrahedra, thus reducing the Si:O ratio to 2:1. If all tetrahedra contained silicon the structure would be electrically neutral, as in quartz (SiO_2), but in zeolites some of the silicon is replaced by trivalent aluminum giving rise to a deficiency of positive charge. This charge is balanced by non-framework mono and divalent cations throughout the structure. Thus the general formula for zeolites is given as:

$$(Li,Na,K)_a\ (Mg,Ca,Sr,Ba)_d\ [Al_{(a+2d)}Si_{n-(a+2d)}O_{2n}] \cdot mH_2O$$

where the part in the square brackets represents the framework atoms and the parts outside are the exchangeable cations and water molecules. Some loosely bound water is always present and can be driven off continuously and reversibly on heating from room temperature to about 350 °C. The cations can be changed by simple washing with different cationic basic solutions; thus some zeolites are used for their ion exchange capacity. In the acid form, with H^+ acting as the charge compensating cation, zeolites are superacids and are very important catalysts for reactions such as catalytic cracking in petroleum refining.

Crystal structure

Open frameworks (spec. grav. = 1.9-2.2 g/cc), void volumes up to 50% and surface areas 500 m^2/g are typical in zeolites. The primary building blocks are SiO_4 and AlO_4 tetrahedra, these link to form regular, simple polyhedra, called secondary building blocks which then link to form the larger framework structure. These secondary building units (shown in figure A.1) distinguish the eight different zeolite structure types. This representation of the structure shows only the tetrahedral atoms and the oxygen is assumed present along the lines connecting the tetrahedral atoms.

Group 1, also known as S4R, uses the single 4-member ring as its secondary building block; naming again only reflects the number of tetrahedral atoms and the number of oxygen atoms is assumed to be twice the number of tetrahedral atoms. The 4-member ring chains can form frameworks by wrapping around square prisms and interconnecting as in analcime.

Zeolites in group 2, S6R, are formed of single 6-member rings. Parallel 6-member rings are linked via tilted 4-member rings and the centers of the 6-member rings pack ABCABC or ABAB, analogous to hexagonal close pack or face centered cubic structures.

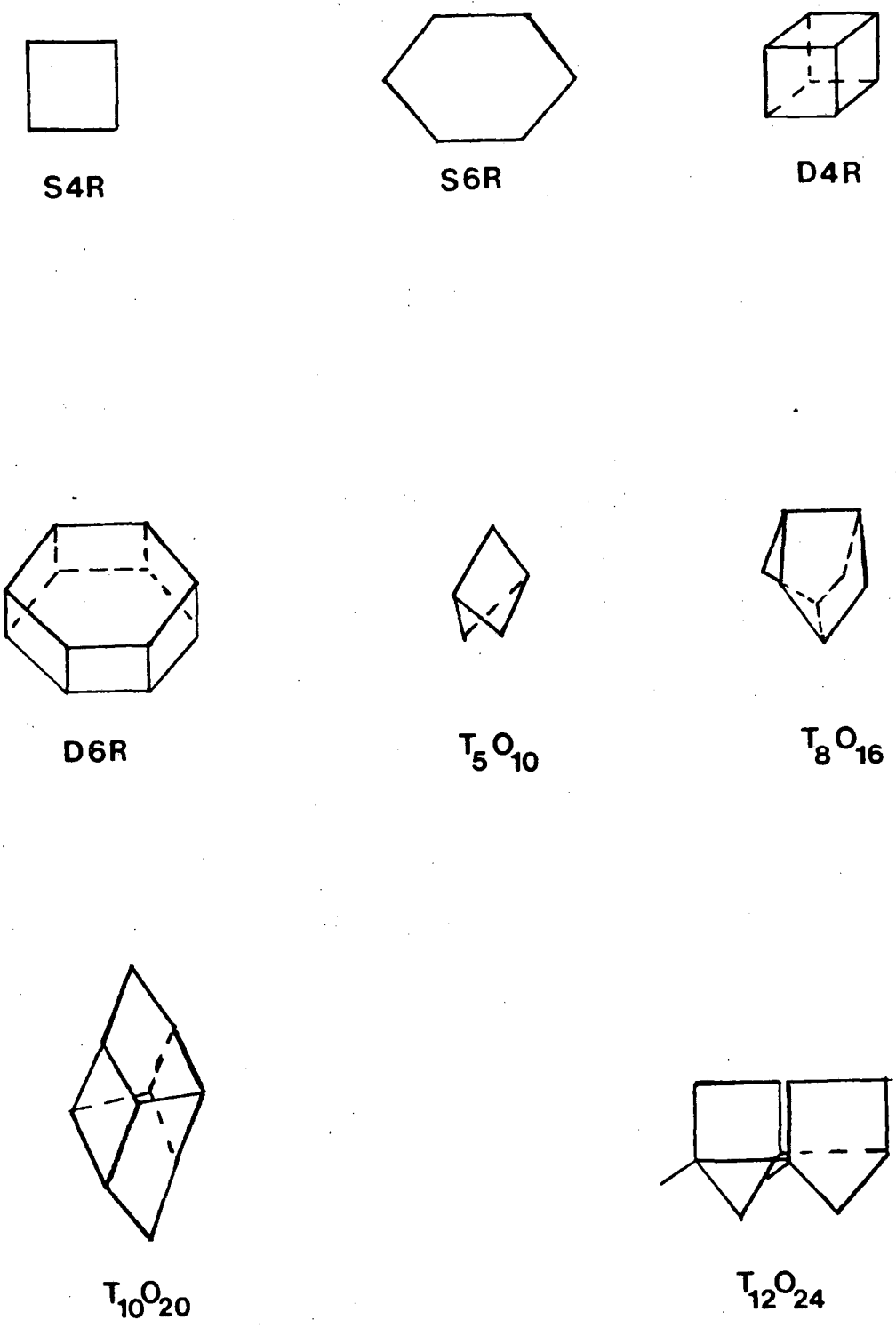

Figure A.1 - The secondary building units for zeolites. The tetrahedral atoms are shown at the vertices of the polygons, the oxygen atoms lie approximately midway between along the connecting lines.

Zeolite erionite packs AABAAC and offretite stacks AABAAB.

Double 4-member rings, D4R, compose group 3. Mazzite is formed of three doubly connected 4-member ring chains around a triad (c-axis) forming a column of gmelinite cages.

Group 4, D6R, uses double 6-member rings as secondary building blocks. These double 6-member ring blocks can stack as the S6R stack; chabazite has D6R ABC stacking or S6R AABBCC stacking, while gmelinite has D6R AB or S6R AABB stacking. The faujasite structure results when D6R are linked to form sodalite cages in a diamond arrangement. Synthetic zeolites X and Y (differing from faujasite only in Si/Al-ratio) have .75 nm pores and are used extensively as cracking catalysts in petroleum refining.

Group 5 is comprised of chains of the T_5O_{10} building unit and for obvious reasons are fibrous zeolites. If the chains link to adjacent chains with mirror symmetry, edingtonite results, whereas if the chains link with rotation symmetry, natrolite is formed.

The secondary building unit of group 6 is a T_8O_{16} unit. These units bond together with mirror symmetry to form the thermally very stable zeolite mordenite.

Group 7 is formed from $T_{10}O_{20}$, heulandite units, from which the group gets its name. These units link into sheets that are only loosely connected thus cleavage is easy.

Synthetic zeolites, ZSM-5 and ZSM-11, which do not exist in nature belong to group 8, the pentasils. Zeolites first synthesized at Mobil Corporation have the ZSM naming scheme, where Z stands for zeolite and SM is for Socony-Mobil, the former name of the Mobil Corporation. The $T_{12}O_{24}$ secondary building blocks, made of two 5-member rings (hence the group name-pentasil), link to form 10-member rings that define the channel openings (fig. A.2). In ZSM-5 the structure is such that (100) slabs are related by inversion, while in ZSM-11 the (100) slabs are mirror images of one another. This difference in

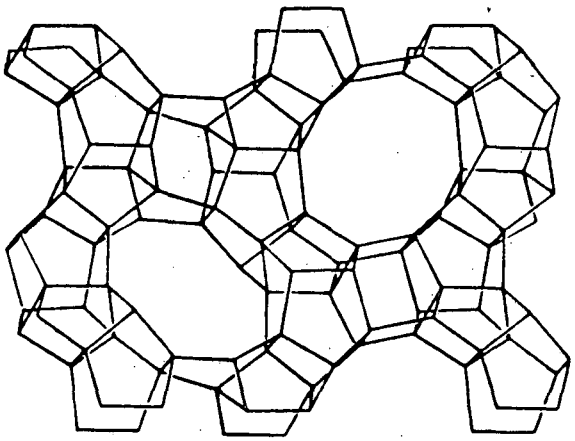

XBL 886-2081

Figure A.2 - Schematic representation of the ZSM-5 framework with the secondary building blocks linked to form 10-member rings defining the pore structure. The orientation is along the 010 straight channels.

symmetry produces two different pore structures. In ZSM-11 there are two straight intersecting channel systems parallel [010] and [100], with the same elliptical opening ($\sim$.51 x$\sim$.54 nm), whereas in ZSM-5 the channels parallel [010] are straight with $\sim$.54 x $\sim$ .56 nm free diameter and the channels parallel [100] are sinusoidal with openings $\sim$.51 x $\sim$.54 nm. This subtle difference in pore structure results in different products when used as catalysts and ZSM-5 generally gives the preferred product distributions.

Zeolite ZSM-5 has become very important as a shape selective catalyst the petroleum industry. Its small pore size prohibits the diffusion of large bulky organic molecules while allowing rapid diffusion of spaghetti-like n-paraffins. These straight chain and singly branched paraffins, making up the heavy waxy fraction of crude petroleum, are selectively cracked into smaller paraffins and olefins. The resulting product consists largely of gasoline of good octane number.

In addition to cracking, the shape selectivity of ZSM-5 has found large scale application in the isomerization of o-xylene and m-xylene to p-xylene. The catalyst isomerizes the three xylenes to equilibrium. Zeolite ZSM-5 is used in a new process, the conversion of methanol to gasoline (MTG). Methanol is converted to dimethyl ether, then to olefins that then form higher olefins and aromatics over ZSM-5. No heavy products are formed, only "gasoline-range" hydrocarbons.

The commercial success of zeolite ZSM-5, in addition to the scientific interest in these materials, drive researchers to synthesize new molecular sieve structure materials such as gallium, boron and iron silicate analogs of zeolites Y and ZSM-5, and the new aluminophosphates and silicon aluminophosphates.

Bibliography

Breck, D.W., "Zeolite Molecular Sieves: Structure, Chemistry, and Use" John Wiley and Sons, Inc., New York, (1974).

Gottardi, G., and Galli, E., "Natural Zeolites," Springer-Verlag, New York, (1985).

Kokotailo, G.T., Chu, P., Lawton, S.L., and Meier, W.M., Nature, **275**, 119 (1978).

Kokotailo, G.T., Lawton, S.L., Olson, D.H., and Meier, W.M., Nature, **272**, 437 (1978).

Mumpton, F.A., "Mineralogy and Geology of Natural Zeolites," (Mumpton, F.A., ed) Mineralogical Society of America, pp. 1-17 (1977).

Olson, D.H., Kokotailo, G.T., Lawton, S.L., and Meier, W.M., J. Phys. Chem., **85**, 2238 (1981).

Smith, J.V., "Zeolite Chemistry and Catalysis," (Rabo, J.A.,ed) American Chemical Society, pp. 3-79 (1976).

APPENDIX B

Appendix B - Olivine standard

The olivine standard and analysis information was provided by J. Donovan of the Earth Science Laboratory at the University of California at Berkeley. Wet chemical analysis, performed by I.S.E. Carmichael, yielded the composition shown in table B.1.

Table B.1 - Analysis of olivine standard, G-94.

oxide	wgt%
FeO	11.97
MnO	0.19
MgO	47.03
CaO	0.24
NiO	0.26
SiO_2	40.31†

† SiO_2 determined by difference.

APPENDIX C

ACKNOWLEDGEMENTS

There are many people who have helped me reach this goal and I would like to take this opportunity to express my gratitude to them.

Professor Ronald Gronsky, my advisor, who supported this and other projects and remained enthusiastic throughout the past five years. Professors Gabor Somorjai and Alan Searcy for reviewing this thesis. Professor Heinz Heinemann for fruitful discussions and encouragement in the later stages of this work.

Rosemarie Szostak and Vinny Nair for preparation, chemical and catalytic characterization of the iron silicate materials used in this study, and for many helpful long distance discussions.

Charles Lyman and Joe Michaels for helpful collaboration in the area of x-ray emissive spectroscopy and use of the VG STEM at Bethlehem Steel Company.

Dave Ackland, Chris Nelson, Chuck Echer, Don Jurica, Don Pardoe and Cyril Gleeson for always providing the necessary technical assistance and for keeping the microscopes in top working order. Caroline Schooley and Doug Davis for maintaining "state of the art" microtomy facilities.

Annemarie Mieke for help in sorting through the many iron oxygen phases.

Jamie Rose for motivating the timely finish of this thesis.

Mike, Byung-Teak, Charlene, Eileen, Eduardo, Roar, Jamie, Dan, Shelly, Mahesh, Hisham, Matt, Lucia, and Larry thanks for some great parties. The Gronsky and Thomas groups for sharing and adding to the experience.

Mike for remaining optimistic and providing help and encouragement throughout the process. Mom and Dad and the whole Csencsits family for their long distance confidence.

This work has been funded by the Director, Office of Energy Research, Office of Basic Energy Sciences, Materials Science Division of the U. S. Department of Energy under Contract No. DE-AC03-76SF00098.

LAWRENCE BERKELEY LABORATORY
TECHNICAL INFORMATION DEPARTMENT
1 CYCLOTRON ROAD
BERKELEY, CALIFORNIA 94720